International Journal of Nanomedicine

Dovepress
Taylor & Francis Group

Open Access Full Text Article

ORIGINAL RESEARCH

Dual-Action Theranostic Nanoparticles Delivering Toll-Like Receptor 2 Inhibitors and Chemotherapy Target Breast Cancer Cells and the Tumor Microenvironment

Antonino Di Lorenzo[1,2,*], Chiara Romiti[1–3,*], Alessandro Amaolo[1,2], Chiara Cossu[1,2], Antonella Iacoviello[1,2], Claudia Curcio[1,2], Marco Forni[2], Cristina Zanini[2], Federica Cavallo[1,2], Giuseppe Ferrauto[1,2], Enza Di Gregorio[1,2,*], Laura Conti[1,2,*]

[1]Department of Molecular Biotechnology and Health Sciences, University of Turin, Turin, Italy; [2]Molecular Biotechnology Center "Guido Tarone", University of Turin, Turin, Italy; [3]Department of Medical Biotechnologies, University of Siena, Siena, Italy

*These authors contributed equally to this work

Correspondence: Enza Di Gregorio; Laura Conti, Department of Molecular Biotechnology and Health Sciences and Molecular Biotechnology Center "Guido Tarone", University of Turin, Turin, Italy, Tel +390116708459; +390116706458, Email enza.digregorio@unito.it; laura.conti@unito.it

Purpose: Breast cancer remains the leading cause of cancer-related death in women, largely due to therapy resistance driven by both tumor-intrinsic and tumor microenvironment (TME)-mediated mechanisms. Toll-like receptor 2 (TLR2), which is overexpressed in breast tumors, promotes cancer progression and chemoresistance through both cancer-cell intrinsic and immune-mediated signaling, making it a promising therapeutic target.

Methods: We developed a targeted therapy combining two types of nanoparticles (NPs) for targeted drug delivery, hybrid poly (lactic-co-glycolic acid) (PLGA)- lipid NPs loaded with the TLR2 inhibitor CU-CPT22 (PLGA-CU) and liposomes encapsulating doxorubicin (LIPO-DOXO). Both NP types were functionalized with cyclic RGD peptides to target $\alpha_v\beta_3$ integrins. Their effects were evaluated in vitro on triple-negative and HER2-positive breast cancer cells and in vivo in 4T1 triple negative breast cancer tumor-bearing mice.

Results: PLGA-CU effectively inhibited TLR2 signaling. Both PLGA-CU and LIPO-DOXO reduced cell viability and induced apoptosis, with stronger effects observed when used in combination. In vivo imaging confirmed the accumulation of NPs in tumors. While monotherapies reduced tumor growth, the combined treatment targeted both cancer cells and TME, leading to reduced angiogenesis and immunosuppression, as well as enhanced anti-tumor activity.

Conclusion: NP-mediated delivery of a TLR2 inhibitor and doxorubicin produces synergistic anti-cancer effects in breast cancer models. This approach may help overcome chemoresistance and improve therapeutic outcomes, offering a promising strategy for the treatment of advanced breast cancer.

Keywords: breast cancer, hybrid PLGA-lipid NPs, immunotherapy, liposomes, magnetic resonance imaging, TLR2 inhibitor

Introduction

Significant progress has been made in the diagnosis and treatment of breast cancer, particularly in Western countries, where routine screening techniques have improved early detection.[1] Additionally, a deeper understanding of breast cancer subtypes has led to the development of more effective therapies, improving patient survival. Nevertheless, breast cancer remains the leading cause of cancer-related deaths in women. The American Cancer Society estimates that in 2025, breast cancer will account for 32% of all cancer diagnoses in women, with 319,750 new cases and 42,680 deaths in the United States alone.[2]

https://doi.org/10.2147/IJN.S556284
Received: 25 July 2025
Accepted: 14 December 2025
Published: 27 February 2026

Graphical Abstract

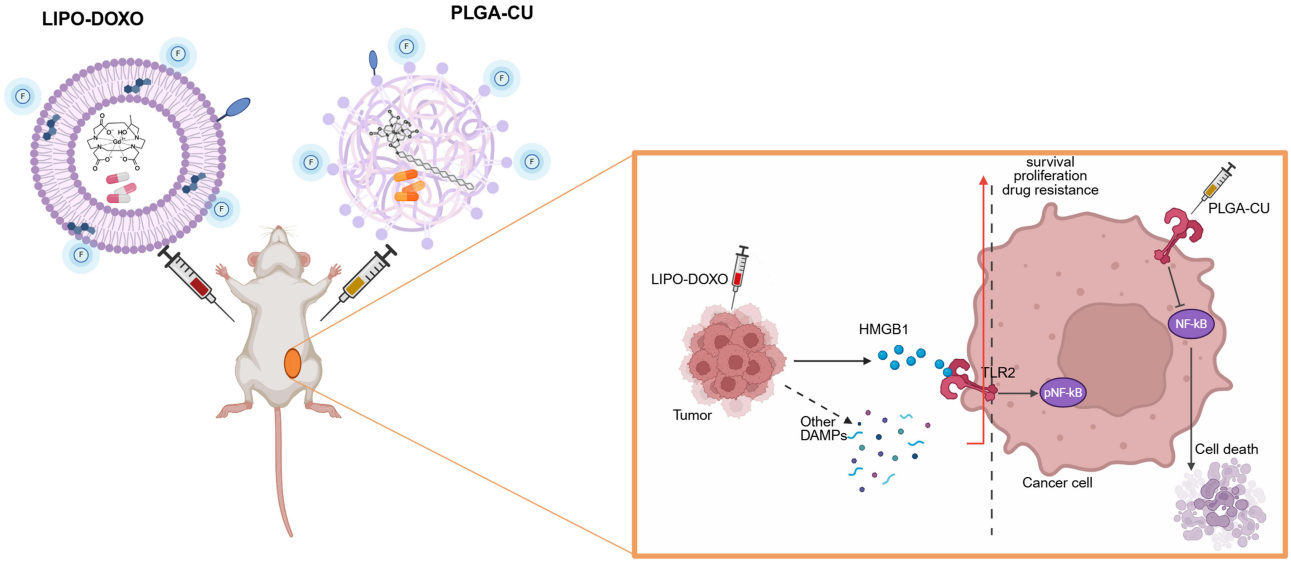

Chemotherapy is widely used as both adjuvant and neoadjuvant therapy, especially in highly proliferative subtypes such as HER2-positive and triple negative breast cancer (TNBC). However, recurrence due to drug resistant tumor cells remains a major challenge, contributing to approximately 90% of cancer-related deaths.[3] Intrinsic resistance mechanisms include alterations in drug targets, reduced drug uptake, increased efflux, activation of survival pathways, enhanced DNA repair, and the presence of cancer stem cells (CSCs).[4] Tumor microenvironment (TME) provides a critical contribution to therapy resistance by controlling the release of cytokines that drive metabolic reprogramming, immune evasion and survival, or by altering drug availability through angiogenesis and extracellular matrix remodeling.[5]

To overcome resistance, therapies must target both cancer cells and the TME. One promising target in this context is Toll-like receptor 2 (TLR2), which is highly expressed in breast tumors and is associated with poor patient prognosis.[6,7] We previously demonstrated that TLR2 is expressed on breast cancer cells and that its activation by damage-associated molecular patterns (DAMPs), such as High Mobility Group Box 1 (HMGB1), triggers NF-κB signaling, promotes CSC self-renewal, enhances tumor growth, and supports cancer cell survival.[8] HMGB1 and other DAMPs are released during chemotherapy-induced immunogenic cell death, suggesting that TLR2 inhibition could enhance chemotherapy efficacy.[6]

In addition to cancer cells, TLR2 is also expressed on immune cells within the TME, where it contributes to immunosuppression. TLR2 activation in macrophages promotes pro-tumoral M2 polarization and recruitment of regulatory T cells (Tregs).[9,10] In Tregs, TLR2 signaling promotes their expansion,[6] while in dendritic cells it increases interleukin (IL)-6 and IL-10 secretion, impairing antigen presentation and T cell activation.[11] In B lymphocytes, TLR2-dependent MAPK activation induces regulatory B cells that inhibit effector T cell function through IL-10 secretion.[12,13] Myeloid-derived suppressor cells (MDSCs) also contribute to immunosuppression upon TLR2 activation.[14,15] Therefore, TLR2 inhibition may help restore an immune-permissive TME.

Clinical trials have revealed the safety and efficacy of TLR2-targeting monoclonal antibodies in hematological malignancies (NCT02363491 and NCT03337451). However, no TLR2 inhibitor has been approved for cancer therapy or tested in clinical trials for solid tumors, and information regarding the use of TLR2 inhibitors in solid cancers remains scarce in the literature. TLR2 is overexpressed in pancreatic cancer cells, and treatment with its inhibitor Robinin, a compound present in the flavonoid fraction of *Vigna unguiculata* leaf, or with the anti-TLR2 neutralizing antibodies OPN-305/Tomaralimab or T2.5, impair pancreatic cancer cell epithelial to mesenchymal transition, migration and in vivo growth.[16,17] Similarly, T2.5 significantly decreased organoid formation and in vivo xenograft growth of head and neck

squamous cell carcinoma.[18] In this scenario, we previously demonstrated that the small-molecule TLR2 inhibitor CU-CPT22 restores chemosensitivity in preclinical breast cancer models, providing direct proofs of the therapeutic benefits achievable by TLR2 targeting in this tumor.[6] Unfortunately, CU-CPT22 poor water solubility and chemical instability significantly limit its clinical applications.[19]

To improve CU-CPT22 delivery while avoiding systemic TLR2 inhibition, in this study we developed tumor-targeted nanosystems. Given CU-CPT22's unfavorable physicochemical properties, hybrid poly (lactic-co-glycolic acid) (PLGA)-lipid NPs were the appropriate nanosystem for this purpose. PLGAs are known for their biocompatibility, low toxicity, controlled drug release, and ability to protect encapsulated drugs from degradation.[20] The presence of PEGylated phospholipids in these hybrid NPs prolongs circulation lifetime and enables easy surface functionalization for targeted delivery.[21] PLGA-based nanosystems are approved by the Food and Drug Administration and by the European Medical Agency for drug delivery.[22] The properties of PLGA-based NPs have made them an ideal substrate for developing versatile drug delivery systems in breast cancer. For instance, a recent study reported the development of PLGA NPs loaded or surface-decorated with the anti-HER2 monoclonal antibody trastuzumab. These NPs, capable of light-triggered local release via an optical fiber system, achieved enhanced cytotoxicity in HER2-positive three-dimensional tumor models.[23] Similarly, trastuzumab-decorated PLGA NPs loaded with paclitaxel were used as delivery systems for breast cancer treatment.[24] These findings reinforce the potential of PLGA NPs for targeted and controlled delivery, providing the rationale for their use in dual-action theranostic strategies. However, to further enhance chemotherapy efficacy and reduce systemic toxicity, we chose to encapsulate doxorubicin in liposomes, which better fit its hydrophilic structure.[25]

The decision to develop two distinct nanosystems is based on the greater flexibility it offers for using them either individually or in combination as well as on the possibility to easily and properly modulate the dosage of the two employed drugs. Both PLGA and liposomal NPs were functionalized with cyclic Arg-Gly-Asp (RGD) tripeptides, which binds integrin $\alpha_v\beta_3$. This integrin is overexpressed on tumor vasculature and breast cancer cells, facilitating migration and invasion through the interactions with extracellular matrix.[26,27] We previously demonstrated that RGD functionalization enhances NP accumulation in breast tumors and improves the efficacy of docetaxel.[28]

Our results demonstrate that CU-CPT22 and doxorubicin-loaded NPs synergistically inhibit tumor growth in preclinical breast cancer models. These findings suggest that TLR2-targeted nanodelivery systems represent a promising strategy for combination therapies aimed at overcoming chemoresistance and improving clinical outcomes in advanced breast cancer.

Materials and Methods

Chemicals and Reagents for NP Synthesis

1,2-distearoyl-sn-glycero-3-phosphoethanolamine-N-[maleimide(polyethyleneglycol)-2000] (ammonium salt) (DSPE-PEG2000-maleimide), 1,2-distearoyl-sn-glycero-3-phosphoethanolamine-N-[methoxy(polyethylene gly-col)-2000] (ammonium salt) (DPPE-PEG2000-methoxy), (1,2-dioleoyl-sn-glycero-3-poshosphoethanolamine-N-(carboxyfluorescein) (ammonium salt) (DOPE-CF) and 2-Oleoyl-1-palmitoyl-sn-glycero-3-phosphocholine (POPC) were purchased from Avanti Polar Lipids Inc. CU-CPT22 was purchased from Tocris Bioscience. Doxorubicin (European Pharmacopoeia Reference Standard), Poly(D,L-lactide-co-glycolide) (50:50, mol wt 30,000–60,000) (PLGA), poly-vinyl-alcohol (*mol wt* 31,000–50,000), cholesterol, trimethylsilyl-propanoic acid (TSP, NMR standard), sodium chloride, methanol, 4-(2-hydroxyethyl)-1-piperazineethane-sulfonic acid (HEPES), sodium acetate, sodium hydroxide, hydrochloric acid, chloroform, nitric acid, 3-(4,5-dimethylthiazol-2-yl)-2,5-diphenyltetrazolium bromide, and all the other chemicals were acquired from Sigma-Aldrich, and used without further purification. Cyclo(-Arg-Gly-Asp-D-Phe-Cys) acetate salt (c(RGDfC) was acquired from Bachem AG. 1,2-distearoyl-sn-glycero-3-phosphoethanolamine-N-Cyanine 5 (Cy5-DSPE) was purchased from BroadPharm.

Gadolinium (Gd)-amphiphilic complex, Gd(III)-DOTAMA$(C_{18})_2$(Gd-DOTAMA) was synthesized as previously reported.[29] The presence of free Gd-ions was checked to be lower than 0.3% mol/mol by the Orange xylenol procedure.[30] The exact concentration of Gd-complex was quantified by a relaxometric approach, as previously reported.[31] ProHance$^{(R)}$ (Gadoteridol) was kindly provided by Bracco Imaging S.p.A. All the chemical structures of the molecules included in the NPs and liposomes formulation are depicted in Figure S1A.

NP Preparation

PLGA NPs (hereinafter named PLGAs) were prepared using the *water-in-oil* emulsion method, as in[28] and CU-CPT22 encapsulation occurred during the self-assembly of the polymeric matrix. Briefly, the organic phase was prepared by dissolving PLGA pegylated phospholipids and all the other components in chloroform. 25 mg PLGA, 1.0 mg 1,2-distearoyl-sn-glycero-3-phosphoethanolamine-N-[methoxy(polyethylene glycol)-2000] (ammonium salt) (18:0 PEG2000 PE) and 1.2 mg 1,2-distearoyl-sn-glycero-3-phosphoethanolamine-N-[maleimide(polyethylene glycol)-2000] (ammonium salt) (DSPE-PEG2000-Maleimide) (AvantiPolar Lipids Inc), were dissolved in chloroform (purity ≥ 99.9%). 2 mg of CU-CPT22 were also dissolved in chloroform for drug-loaded NPs, hereinafter named PLGA-CU. The water phase was a 3% PVA aqueous solution. The organic phase was gently dropped into the aqueous phase, in ice. Sonication was performed with an immersion-tip instrument in 2 cycles of 1.5 min each, 70% power amplitude. Evaporation of the organic solvent from the oil/water emulsion was carried out for 2 h under vacuum-rotation at room temperature. PLGAs were purified with dialysis against fresh HEPES/NaCl buffer (3.8 mM HEPES, 0.15 mM NaCl, pH 7.2±0.2, 280±20 mOsm/L) and ultrafiltered through centrifugation (4°C, 5500 rpm) in Vivaspin® tubes (10'000 MWCO) to wash the remaining PVA and concentrate the PLGA to the wanted volume.

Liposomes were obtained through lipidic thin-film hydration and solvent evaporation. Briefly, each formulation contained 72% POPC, 25% cholesterol, 1.5% 18:0 PEG2000 PE, and 1.5% DSPE-PEG2000-Maleimide (mol/mol ratio), for a total lipid concentration of 30 mg/mL Cholesterol and phospholipids were dissolved in chloroform and transferred to a round-bottom flask for solvent evaporation under vacuum-rotation to create a monolayered lipidic film. This was subsequently hydrated with ammonium sulfate 0.12 M, pH 5.5 at 55°C to create spontaneous multilamellar vesicles, then extruded through 400 nm and 200 nm-cutoff membrane pores to form a monodispersed suspension with liposomes below 200 nm.

Doxorubicin (hydrochloric salt) incorporation in the internal liposome aqueous phase was done by incubating 0.04 mol of drug per 1 mol of phospholipids, for 1 h at 55°C as in[25,32] to generate LIPO-DOXO NPs.

Unbound drug was washed out through overnight dialysis in the acetate buffer 0.15 M, pH 6.6 ± 0.2.

Both NPs were bound to cyclic RGD peptide[26] through a surface ligation reaction to target $\alpha_v\beta_3$ integrins as in,[28] (Figure S1B). A batch of untargeted NPs (not conjugated to RGD) was prepared as a control.

For PLGAs and liposomes used for the biodistribution studies, 0.17 mg of DSPE-Cy5 were added to the organic phase. For nanosystems applied for Magnetic Resonance Imaging (MRI) and Inductively Coupled Plasma Mass Spectrometry (ICP-MS), 3.2 mg Gd-DOTAMA were added to the chloroform-phospholipids solution during the synthesis of PLGAs, and 0.3 M ProHance(R) in H_2O was used to hydrate the liposome lipidic film. Gd-DOTAMA is an amphiphilic complex with a hydrophobic chain that can be easily embedded in the PLGA matrix, while ProHance is more likely to stay within the aqueous environment of the liposomes core.

NP Characterization

Physicochemical properties (size, ζ-potential) were determined by Dynamic Light Scattering (DLS) using Malvern Zetasizer Nano Series DLS instrument, upon diluting NPs 1:100 in filtered HEPES/NaCl buffer. The amount of encapsulated drug was measured through UV/vis absorbance spectroscopy for doxorubicin (using a Janwey 6315 UV/vis spectrophotometer) and high resolution ^{1}H-NMR spectroscopy for CU-CPT22 (using a Bruker NMR spectrometer operating at B0=14T) (Figure S2).

The stability of PLGA and liposomes NPs was tested in vitro either in presence of HEPES/NaCl buffer or in presence of serum albumin (0.6 mM human serum albumin, Seronorm, Sero, As, Norway) at 37°C for a continuous time of 8 days. To obtain this information, Gd-labelled PLGA and liposome NPs synthesized as above were diluted in HEPES/NaCl or in HSA solution and longitudinal water proton relaxation time (T_1) measured for 7−8 days by using Stelar SpinMaster relaxometer (Stelar), operating at 21 MHz (Proton Larmor Frequency). Incubation temperature was monitored to be fixed at 37°C. Data were normalized for Gd-concentration and reported as r_{1p} (Figure S3A and B).

Moreover, the stability of NPs was also monitored by measuring the hydrodynamic radius for 8 days by DLS (in HEPES/NaCl or human serum albumin, 37°C) (Figure S3C and D).

Finally, the kinetics of drug release over time were monitored in vitro for both CU-CPT22-loaded PLGA NPs and for doxorubicin-loaded liposomes. For this experiment, 1 mL of each NP was loaded inside dialysis bags and placed in dialysis versus 40 mL of HEPES/NaCl buffer (pH 7.4, 4°C). At different time points (up to 82 h) an aliquot of specimens was collected and used for quantification of the retained drug (by NMR for CU-CPT22 and by UV/vis absorbance for doxorubicin, as above reported). After each sampling, the buffer is replaced with fresh one (Figure S4A and B).

Cells

4T1 and MDA-MB−231 TNBC cell lines were obtained from the American Type Culture Collection in 2018, stored and cultured as reported [6] The HER2$^+$ WT-874 breast cancer cell line was generated and cultured as in Di Lorenzo et al[6] bEnd.3 cells were kindly provided by Dr. F. Pericle (Immunogenesis Inc). All cell lines were tested negative for mycoplasma as reported.[33]

3-(4,5-Dimethylthiazol-2-Yl)-2,5-Diphenyltetrazolium Bromide (MTT) Assay

WT-874 or 4T1 cells (5×10^3) were cultured overnight in 96-well plates. Scalar doses of CU-CPT22, doxorubicin, PLGA-CU, LIPO-DOXO or of the empty NPs were then added. In parallel experiments, cells were treated with recombinant mouse IL-6 (Peprotech, 20 ng/mL) or with the TLR2 agonist PGN-SA (200 μg/mL). After 48 h, cell viability was assessed using the MTT assay.[6]

Tumorsphere-Generation Assays

Tumorspheres were generated from cell lines as in,[8] 24 h later, cells were treated with IL-6 (20 ng/mL) or 200 mg/mL PGN-SA or left untreated. After four days, contrast phase images were acquired (10X) and the number of spheres counted (4X) using Zeiss Axio Observer or Leica DMi1 inverted microscope connected to DC120 digital camera.

Flow Cytometry (FACS)

To evaluate TLR2 expression, exponentially growing 4T1 or WT-974 cells were detached and stained with a PE-conjugated anti-TLR2 monoclonal antibody (Biolegend) as in.[6] To assess uptake, WT-874 and 4T1 cells were incubated with 5 μM FITC-containing PLGA-CU or untargeted PLGA-CU for 4 h at 37°C. In parallel experiments, cells were incubated with 5 μM FITC-containing PLGA-CU for 1 h at 37°C or 4°C. After washing, aliquots of cells were stripped with an acidic buffer to remove surface-bound PLGA, then all samples were analyzed by FACSVerse.[28]

To evaluate CSC markers, tumorspheres were treated with IL-6 (20 ng/mL) or 200 μg/mL PGN-SA or left untreated and stained with PE-conjugated anti-TLR2 monoclonal antibody (Biolegend) as in.[6] In all assays, propidium iodide was added to exclude dead cells. To analyze cell apoptosis, 4T1, WT-874, and bEnd.3 cells were treated for 48 h with either 1 μM doxorubicin or LIPO-DOXO, and 5 μM CU-CPT22 or PLGA-CU, administered individually or in combination, either as free drugs or in NP form. Then, cells were stained with Annexin V-Apoptosis Kit-APC (eBioscience). To analyze NF-κB activation, cells were either treated as for apoptosis or PGN-SA (200 μg/mL) alone and in combination with 5 μM CU-CPT22 or PLGA-CU for 24 h and stained as in.[6] To analyze tumor infiltrate and CSC frequency, tumors were processed and stained as in Conti et al.[8] Samples were acquired on a BD-FACSVerse and analyzed with FlowJO10.5.3. The CD45$^+$ leukocytes and CD45$^-$ cells were gated, and cell populations analyzed as follows: NK: CD3$^-$ CD49b$^+$; CD4$^+$ T cells: CD3$^+$ CD49b$^-$ CD4$^+$; CD8$^+$ T cells: CD3$^+$ CD49b$^-$ CD8$^+$; M1 macrophages: CD11b$^+$ F4/80$^+$ MHC-II$^+$; M2 macrophages: CD11b$^+$ F4/80$^+$ CD206$^+$; CSCs: CD45$^-$Sca1$^+$, CD45$^-$ CD44$^+$ CD24$^-$.[6]

Western Blot

Cells were lysed for protein extraction using a Triton lysis buffer (50 mM Tris-HCl pH 7,6, 120 mM NaCl, 1% Triton X-100) supplemented with 1 mM Phenylmethylsulfonyl fluoride, 1 mM Sodium orthovanadate, 1 mM Sodium fluoride and protease inhibitors cocktail (Sigma-Aldrich) for 20 min on ice. Samples were scraped and collected and then centrifuged for 10 min at 14.000 g. Supernatants containing proteins were harvested and quantified using the Pierce™ BCA Protein Assay Kit (Thermo-Fisher Scientific). Proteins were diluted with Laemmli loading buffer 4X (BioRad) + β-mercaptoethanol (1:10 *vol/vol*) to reach the concentration of 1 μg/μL and then boiled at 95°C for 10 min. 40 μg of proteins were subsequently separated in a 4–20% polyacrylamide Precast Gel Mini-PROTEAN TGX (BioRad), then

transferred to a polyvinylidene fluoride membrane. Non-specific binding sites were blocked using 5% non-fat milk (Santa Cruz Biotechnology) in Tris-buffered saline supplemented with 0.1% Tween 20), 1 h at room temperature. The membranes were incubated with mouse anti-vinculin (produced in-house, 1:8000), rabbit anti-NF-kB (D14E12, Cell Signaling Technology, 1:5000), rabbit anti-phospho NF-kB p65 (Ser 536, 93H1, Cell Signaling Technology, 1:5000), overnight at 4°C, followed by incubation with HRP-linked goat anti-mouse (#A0545, Sigma-Aldrich, 1:2000) or with HRP-linked goat anti-rabbit (#A4416, Sigma-Aldrich, 1:2000 or 1:300000) for 1 h at room temperature. The signals were detected by reaction with HRP substrate (Westar ECL substrate Antares #XLS0142, or Hypernova #XLS149, Cyanagen) and images were acquired using a Chemidoc TM Touch Imaging System (Bio-Rad).

ELISA

Cells were treated with 5 μM CU-CPT22 or equivalent PLGA-CU and 2 μM doxorubicin or equivalent LIPO-DOXO, either individually or combined as for the apoptosis. Supernatants were harvested after 48 h, and IL-6, tumor growth factor β (TGF)- β and vascular endothelial growth factor (VEGF) were quantified by using ELISA (R&D Systems).

In vivo experiments

Mice were bred and housed in pathogen- and saprophyte-free conditions at the animal facility of the Molecular Biotechnology Center "Guido Tarone" in accordance with institutional guidelines and the "Directive 2010/63/EU on the protection of animals used for scientific purposes" european guidelines. The study protocol was approved by the Animal Care and Use Committee of the University of Turin and the Italian Ministry of Health (authorization N° 10/2023-PR; CC652.191 and CC652.191.EXT.74; 469/2021-PR; CC652.154). All mice were fed *ad libitum* with the Special Diet Services complete universal vegetal diet for rats, mice and hamsters (code DS811910G10R), containing wheat, extruded soybeans, barley, wheat bran, soybean meal produced from genetically modified soybeans, calcium carbonate, dicalcium phosphate, sodium chloride, pre-mixture of vitamins and minerals, DL methionine.

4T1 cells (1×10^4/mouse) were orthotopically injected into the fourth mammary glands of 7-8-weeks old female BALB/c mice. To analyze NP biodistribution and pharmacokinetics, mice were analyzed 21 days post-injection, when tumors reached an average volume of 100 mm^3. To setup the therapeutic protocols, when tumors reached an average volume of 10 mm^3, mice were blindly randomized and treated intraperitoneally (i.p.) with vehicle (0.25 mL HEPES/NaCl solution, control), 2.5 mg/kg PLGA-CU or 5 mg/kg PLGA-CU. In parallel experiments, mice were treated with vehicle or PLGA-CU not conjugated to RGD or with LIPO-DOXO (3 mg/kg) with or without RGD. To evaluate PLGA-CU and LIPO-DOXO combination, once tumors reached 10 mm^3 mean volume, mice were blindly randomized into four treatment groups, receiving i.p.: vehicle (control), 5 mg/kg PLGA-CU, 3 mg/kg LIPO-DOXO, or both PLGA-CU and LIPO-DOXO. In all experiments, treatments were administered twice weekly for two weeks (4 treatments in total). Mice were monitored daily for signs of distress. Tumor diameters were measured twice a week using an electronic caliper and sacrificed when tumors in controls reached an average volume of 500 mm^3. One day after the final treatment, mice were analyzed by MRI, then they were euthanized, lungs and tumors were excised, weighed, fixed in 4% formaldehyde, and processed for histological analysis. Lungs metastases were analyzed as in.[34] BALB-neuT mice[35] were treated once per week intravenously (i.v.) with either 2 mg/kg doxorubicin, 2 mg/kg LIPO-DOXO or vehicle for a total of seven weeks, starting when the first tumor became palpable (at 15–17 weeks of age). Tumor size was measured weekly using a caliper.

Immunohistochemistry (IHC)

Peroxidase activity was inhibited in 3 μm-thick slices derived from formalin-fixed and paraffin-embedded tumors by incubation in 3% hydrogen peroxide aqueous solution for 10 min. Samples were pre-treated by microwave antigen retrieval using EDTA buffer, citrate pH 6 (Dako) and incubated with anti-CD31 antibody (Abcam, Cat#ab182981, 1:2000) for 30 min at room temperature. The rabbit EnVision system (Dako) was used before diaminobenzidine tetrahydrochloride (Dako) incubation. Sections were counterstained with hematoxylin before dehydration and mounting. Slides were digitized with the Panoramic Desk scanner and subsequently evaluated by a pathologist with Panoramic Viewer (both from 3D HISTECH), and the presence of positive cells was quantified with QuPath0.5.1.[36]

Magnetic Resonance Imaging

Mice underwent MR imaging at 7.1 T using a Bruker Avance300 spectrometer equipped with a Micro2.5 microimaging probe. T_2-weighted (T_{2W}) morphological images were acquired with a standard Rapid Acquisition with Refocused Echoes (RARE) sequence with the following imaging parameters: repetition time (TR) = 4000 ms, echo time (TE) = 40.57 ms, RARE factor = 24, flip angle = 180°, signal averages = 4, field of view (FOV) = 30×30 mm, matrix size = 256 × 256, spatial resolution = 0.117×0.117 mm per pixel, slice thickness = 1 mm).[28]

For Chemical Exchange Saturation Transfer (CEST) and Amide Proton Transfer (APT)-MRI analysis, a typical RARE sequence was used (TE=3 ms, TR=5 s) with isotropic 64×64 acquisition matrix, FOV= 1 cm, slice thickness =1 mm (NEX = 2, RARE Factor = 16). The whole sequence was preceded by a saturation scheme consisting of a continuous rectangular wave pulse 1.5 s long with a RF intensity typically corresponding to B_1=3 μT (other B_1 powers were tested and 3 μT was chosen as good compromise between enough signal and low direct water saturation). A frequency offset range of ±20 ppm was investigated. The Z-spectra were interpolated by smoothing splines to identify the *zero-offset* on a *pixel-by-pixel* basis of the *bulk* water and then to assess the correct ST % value over the entire range of frequency offsets investigated. Custom-made software, compiled in the Matlab platform (Mathworks Inc.), was used. The extent of CEST effect was calculated as follows:

$$ST\% = \left(1 - \frac{M_S}{M_0}\right) \times 100$$

where Ms is the intensity of the *bulk* water NMR signal after irradiation on resonance of the mobile proton pool and M_0 is the intensity of the *bulk* water NMR signal after irradiation at -Δω. The analysis was carried out at two different chemical shifts, i.e. Δω= 2 ppm and Δω= 3.4 ppm. The first resonance is related to the $CEST_{@2ppm}$ signal,[37,38] typical of creatine and other amine-containing metabolites. The second resonance is related to amide protons of polypeptides (i.e. Amide Proton Transfer, APT, MRI). The $CEST_{@2ppm}$ signal arises from exchangeable protons of intracellular creatine and other generic amines and has been shown to correlate linearly with creatine levels.

$CEST_{@2ppm}$ signal is also influenced by pH, so the AACID (Amine and Amide Concentration Independent Detection) CEST-MRI sequence[39] can be used to non-invasive tumor pH measurement. AACID values reflect the ratio between the 3.5 ppm amide and 2.0 ppm amine CEST effect within physiological pH ranges.

Optical Imaging

Optical imaging was performed with the IVIS Spectrum small animal imaging system (PerkinElmer) using a customized filter set, exciting at both 480 and 620 nm and acquiring at 670 nm. Excitation at 480 was used to evaluate the background, and at 620 nm to assess the probe-specific signal. Identical illumination settings (f-stop/field of views/binning/acquisition time, 2/12.5/medium/0.5 s) were used for all samples, using Living Image Software 4.7 (PerkinElmer). Mice bearing 50–100 mm^3 4T1 tumors in both 4th mammary glands were injected i.p. with 230 μL PLGA-CU or 150 μL LIPO-DOXO containing 1 nmol Cy5, anesthetized with 2.5% isoflurane, and analyzed after 5–15-30-60 min, 4 and 24 h (n = 6 for each time point). Regions of interest (ROI) were designed on tumors and muscles, and fluorescence emission normalized to average radiant efficiency (p/s/cm^2 /sr)/(μW/cm^2). For biodistribution studies, mice were sacrificed 24 h post injection, organs were explanted, washed in PBS, and analyzed.

ICP-MS

To measure NP accumulation in tumors, mice bearing 50–100 mm^3 4T1 orthotopic tumors were injected i.p. with PLGA-CU or LIPO-DOXO containing Gd-DOTAMA or ProHance, respectively. After 4 or 24 h, animals were sacrificed and tumors were explanted, weighed, and processed for ICP-MS analysis as in Di Gregorio et al.[40] Briefly, 0.5 or 1 mL of concentrated HNO_3 (70%) was added and, after complete dissolution of the tissue, tumors and organs were further digested by applying microwave heating (MicroSYNTH, Microwave labstation equipped with an optical fiber temperature control and HPR-1000/6M high-pressure reactor, Milestone). After digestion, ultrapure water was added up to 3 mL, then samples were filtered with 0.45 μm filter and analyzed by ICP-MS for quantification of Gd^{3+}, using a Thermo Scientific ELEMENT 2 ICP-MS-Finnigan, Rodano (MI). A calibration curve prepared using four Gd absorption standard solutions in the range 0.005–0.1 μg/mL (Sigma-Aldrich) was used to quantify Gd in the samples, which was expressed as μg of Gd^{3+}/g of tissue.

Statistical Analysis

Statistical significance was evaluated using GraphPad10 software (Dotmatics, MA, USA). Differences in MTT, FACS, IHC, optical imaging, MRI and ELISA data were analyzed using One-way ANOVA. Differences in tumor growth were analyzed using Two-way ANOVA with Bonferroni post-test. All values are reported as means ± standard error of the mean (SEM). $P < 0.05$ was considered significant.

Results

Preparation and Physicochemical Characterization of NPs

Hybrid PLGA-lipid NPs and liposomes (LIPOs) were prepared and tested both in vitro and in vivo. Two separate batches were produced: the first contained Gd-complexes for MRI detection and was used for NPs characterization and in vivo biodistribution studies. The second batch was designed for therapeutic evaluation and contained the TLR2 inhibitor CU-CPT22 (in PLGAs) and doxorubicin (in LIPOs). All NPs were co-loaded with a fluorescent amphipathic probe for in vivo fluorescence imaging and functionalized with PEGylated phospholipid to confer stealth properties. A schematic representation of the NP formulation and the chemical structures of the components are shown in Figure 1 and S1A, respectively. These NPs act as a stealth theranostic system, allowing dual detection by both optical imaging and MRI.

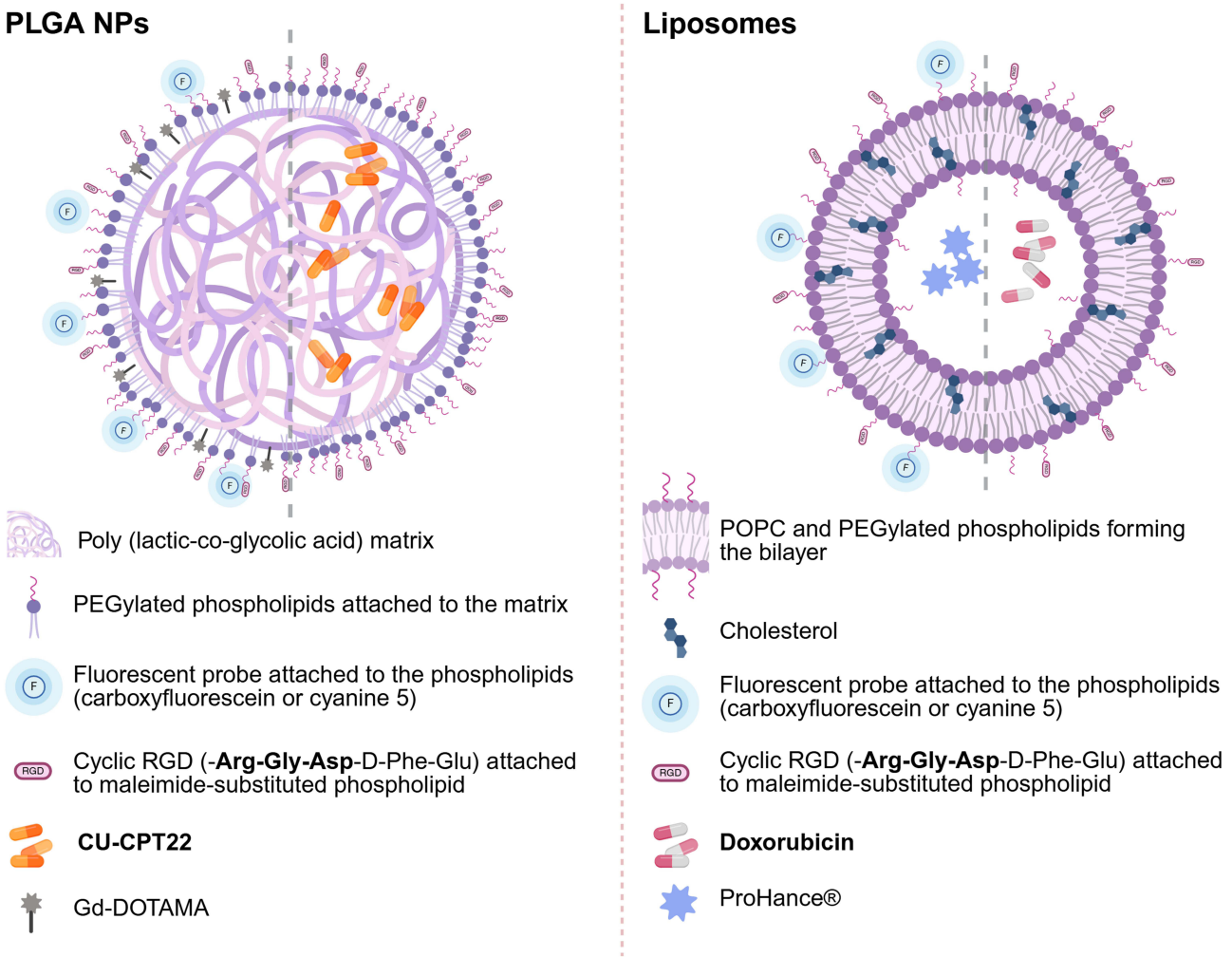

Figure 1 Schematic representation of the NP formulations. The PLGA NPs (left) consist of a PLGA matrix with embedded PEGylated phospholipids, some functionalized with a maleimide moiety for conjugation with targeting cyclic RGD peptides. The system also incorporates the therapeutic agent CU-CPT22, fluorescent probes (carboxyfluorescein or cyanine 5), and the MRI contrast agent Gd-DOTAMA. The liposome formulation (right) features a lipid bilayer formed by POPC and PEGylated phospholipids, also functionalized with maleimide moieties for cyclic RGD conjugation. Cholesterol is included to modulate membrane stability. Doxorubicin is encapsulated as the therapeutic agent, while fluorescent probes and the MRI contrast agent Prohance are integrated for imaging purposes.

PLGAs were prepared using a classic *oil-in-water* emulsion solvent extraction method[41] with the addition of the CU-CPT22 in the organic phase. LIPOs were prepared by using the method of hydration of thin lipidic film after the organic solvent evaporation. Doxorubicin was subsequently loaded using pH gradient method.[25] The chemical components used for PLGA formulation are reported in Figure S1A, while the scheme of RGD conjugation is shown in Figure S1B. A summary of NPs composition and physicochemical properties is presented in Table 1. Both NP types exhibited suitable characteristics for cellular and in vivo applications, with a hydrodynamic diameter of approximately 199±35 nm, a slightly negative ζ-potential (−2.5±0.65 mV), and a polydispersity index (PDI) below 0.2, indicating good size uniformity. Encapsulation efficiency varied between the two NP systems: approximatively 30% for CU-CPT in PLGA and around 60% for doxorubicin in LIPOs (Figure S2). These differences are attributed to the distinct physicochemical properties of the drugs, the NP types, and the respective loading techniques. The stability of both nanoformulations was tested in vitro in HEPES/NaCl buffer or in serum at 37°C. No significant change in the r_{1p} of the Gd-labelled NPs was noted (Figure S3A and B) Analogously, no change in hydrodynamic radius has been detected (Figure S3C and D) Both data confirm the in vitro stability of both NPs both in buffer and in serum.

The kinetics of drug release from NPs were assessed for both systems. Data reported in Figure S4A and B show that CU-CPT22 is quickly released by PLGA NPs whereas doxorubicin is maintained inside the liposomes for longer time (at three days, more than 80% is retained inside the liposomes).

PLGA-CU Effectively Targets Cancer Cells and Inhibits TLR2 Signaling

The functional properties of RGD-targeted PLGAs encapsulating CU-CPT22 (PLGA-CU) were tested in vitro on murine TNBC 4T1 and $HER2^+$ WT-874 cells, both expressing TLR2 and integrin $\alpha_v\beta_3$ (Figure 2A). The NPs were decorated with the cyclic RGD moiety, which has been largely reported to bind $\alpha_v\beta_3$ integrin overexpressed in several solid tumors.[26,28,42,43]

To further confirm that RGD improves cellular uptake of NPs, cells were incubated with FITC-labeled PLGA-CU for 4 h at 37°C. Cells treated with RGD-functionalized PLGA-CU exhibited stronger signal intensity compared to those exposed to untargeted PLGA in both 4T1 and WT-874 cell lines (Figure 2B). This suggests that RGD targeting enhances PLGA NP uptake in breast cancer cells, potentially overcoming the limited endocytosis associated with non-targeted formulations. Then, to further assess NP internalization, cells were incubated with FITC-labeled PLGA-CU for 1 h at either 4°C or 37°C. Surface-bound PLGAs were removed with an acidic incubation, then cells were analyzed by FACS analysis. At 4°C, both treated cell lines showed a higher FITC signal than controls, indicating surface binding. At 37°C,

Table 1 Composition and Characteristics of Multifunctional PLGAs and Liposomes

Name	PLGA-CU	PLGA-Cy5-Gd	LIPO-DOXO	LIPO-Cy5-Gd
Formulation	PLGA, DSPE-PEG2000 maleimide, DPPE-PEG2000-methoxy, c(RGDfC), **CU-CPT22**.	PLGA, DSPE-PEG2000 maleimide, DPPE-PEG2000-methoxy, c(RGDfC), **DSPE-Cy5, Gd-DOTAMA**.	POPC, Cholesterol, DSPE-PEG2000 maleimide, DPPE-PEG2000-methoxy, c(RGDfC), **Doxorubicin Hydrochloride**	POPC, Cholesterol, DSPE-PEG2000 maleimide, DPPE-PEG2000-methoxy, c(RGDfC), **DSPE-Cy5, ProHance**.
Hydrodynamic diameter (nm)	163.1	234.3	195.1	209.3
PDI	0.123	0.218	0.098	0.124
ζ potential	−3.15	−1.93	−2.74	−2.05
Relaxivity (mM^{-1} s^{-1}) at 21.5 MHz, 25°C	/	26.42	/	2.43
Number of Gd/NP	/	$1.1 \times 10^5 \pm 0.2 \times 10^5$	/	$2.3 \times 10^5 \pm 0.3 \times 10^5$
Drug encapsulation efficiency (EE%)	30.0%	/	62.2%	/

https://doi.org/10.2147/IJN.S556284

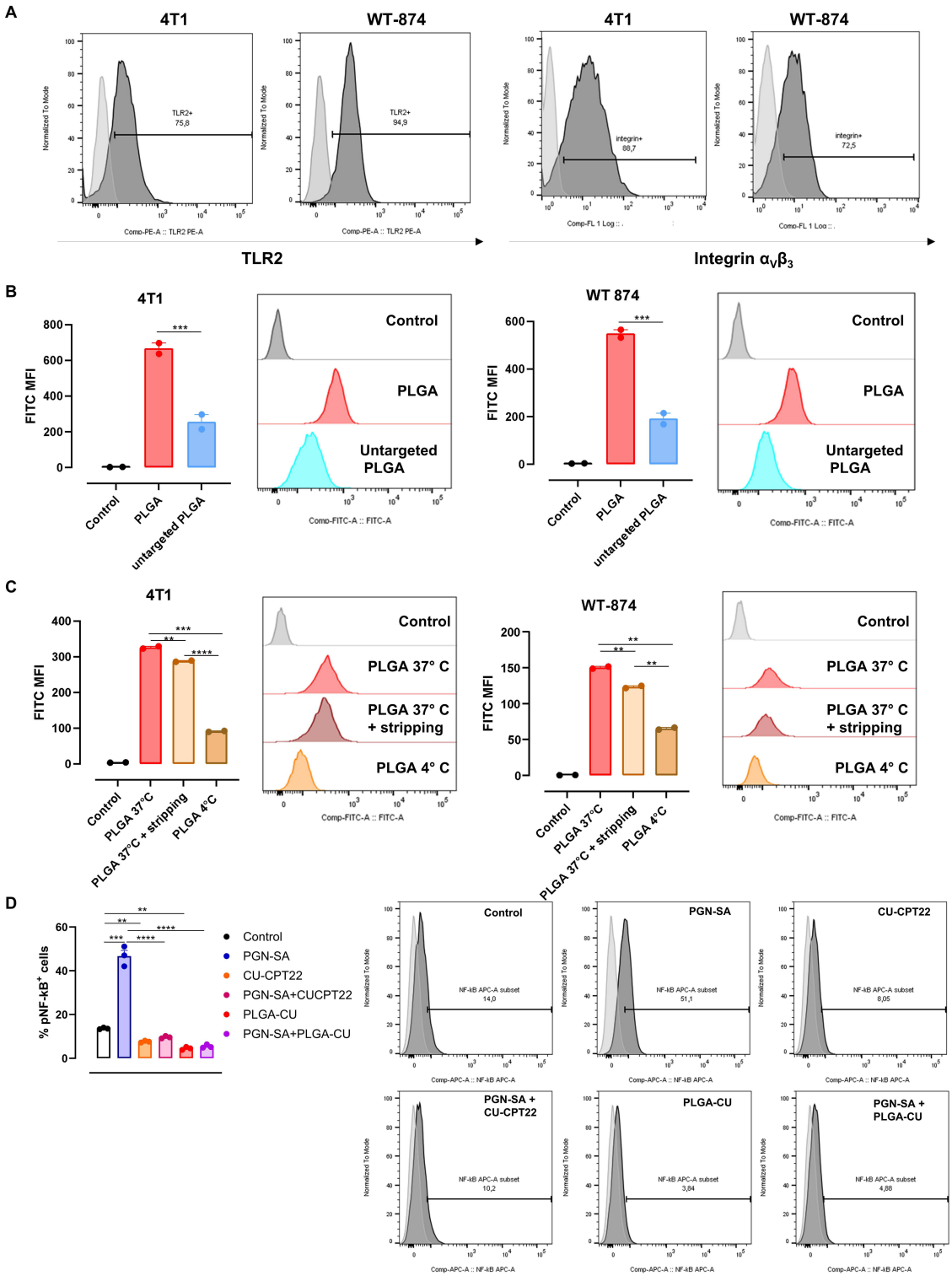

Figure 2 PLGA-CU inhibits TLR2 signaling. (**A**) Representative FACS histogram of the expression of TLR2 and $\alpha_v\beta_3$ integrin on 4T1 and WT-874 cells. Light grey histograms show the background signal obtained by staining cells with an isotype control antibody; dark grey histograms show the signal obtained by staining with the specific monoclonal antibodies. (**B**) FACS analysis of PLGA-CU internalization into 4T1 and WT-874 cells incubated for 4 h at 37° C with 5 μM FITC-containing PLGA-CU or untargeted PLGA-CU, ie PLGA-CU not decorated with RGD. The graphs report the individual values and means ± SEM of the FITC MFI measured from two independent experiments. Representative FACS histograms are shown. (**C**) FACS analysis of PLGA-CU internalization into 4T1 and WT-874 cells incubated for 1 h at 37° C or 4° C with 5 μM FITC-containing PLGA-CU. An aliquot of cells was subjected to acidic stripping to remove membrane-bound PLGA-CU before analysis. The graphs report the individual values and means ± SEM of the FITC MFI measured from two independent experiments. Representative FACS histograms are shown. (**D**) FACS analysis of p65 NF-κB phosphorylation in WT-874 cells treated with PGN-SA (200 μg/mL) ± 5 μM CU-CPT22 or PLGA-CU for 24 h or left untreated. The individual values and means ± SEM of mean fluorescence intensity (MFI) from three independent experiments are reported, as well as representative FACS histograms where light grey histograms show the signal obtained with an isotype control antibody, dark grey histograms with the specific monoclonal antibody. **P < 0.01; ***P < 0.001, ****P < 0.0001, One-Way ANOVA.

signal intensity increased, suggesting intracellular uptake. Acidic wash at 37°C partially reduced the signal, confirming predominant internalization with some residual surface binding (Figure 2C).

Since TLR2 activation in breast cancer cells induces NF-kB phosphorylation, PLGA-CU's ability to inhibit TLR2 signaling was tested. WT-874 cells were treated for 4 h with 5 μM PLGA-CU or free CU-CPT22, then NF-kB phosphorylation (p-NF-kB) was analyzed by FACS. As a positive control, cells were treated with the TLR2 agonist PGN-SA (200 μg/mL), either alone or in combination with PLGA-CU or CU-CPT22. PGN-SA increased p-NF-kB levels, an effect that was abolished by both PLGA-CU and CU-CPT22 (Figure 2D), indicating that PLGA-CU inhibits TLR2 signaling as effectively as the free drug. This is partly due to the release of the drug and partly to the inhibition of intracellular TLR2 signaling.

PLGA-CU and LIPO-DOXO Impair Breast Cancer Cell Viability and Induce Apoptosis

To assess whether PLGA-CU retains the anti-proliferative effects of free CU-CPT22, WT-874 and 4T1 cells were treated with increasing concentrations free CU-CPT22, or empty PLGAs, and cell viability was measured by MTT assay after 48 h. Empty PLGA showed no significant effect except at the highest concentration, which slightly reduced viability (Figure 3A). CU-CPT22 reduced viability, particularly in 4T1 cells, while PLGA-CU exhibited a stronger effect, especially at higher concentrations (Figure 3A). At 5 μM, PLGA-CU significantly reduced viability, whereas free CU-CPT22 did not (Figure 3B), indicating enhanced efficacy through encapsulation. Next, 4T1 and WT-874 cells were treated for 48 h with increasing concentrations of LIPO-DOXO, free doxorubicin, or empty LIPOs. While empty LIPOs had no effect, both LIPO-DOXO and free doxorubicin reduced viability, with LIPO-DOXO being more effective at lower concentrations, especially in 4T1 cells, suggesting improved drug delivery (Figure 3C). At 1 μM, LIPO-DOXO significantly reduced 4T1 viability, whereas free doxorubicin did not. In WT-874 cells, both treatments were effective (Figure 3D).

To further evaluate the individual and combined effects of PLGA-CU and LIPO-DOXO, apoptosis was measured following 48 h treatments with the NPs alone or in combination and compared to free drugs. In 4T1 (Figure 3E) and WT-874 (Figure 3F) cells, PLGA-CU or CU-CPT22 (5 μM) induced a slight increase in apoptosis compared to controls. Both LIPO-DOXO and free doxorubicin (1μM) triggered significant apoptosis. Combining CU-CPT22 with free doxorubicin further enhanced apoptosis relative to single treatments. Notably, PLGA-CU + LIPO-DOXO combination induced significantly higher apoptosis than the free drug combination, reaching ~90% in both cell lines (Figure 3E and F). To enhance translational relevance, this combination was also tested on human TNBC MDA-MB-231 cells. PLGA-CU, LIPO-DOXO, and free doxorubicin significantly increased apoptosis, while CU-CPT22 alone had no significant effect (Figure 3G). CU-CPT22 + free doxorubicin combination slightly increased apoptosis, whereas LIPO-DOXO + PLGA-CU induced a marked increase over single treatments, confirming this NP combination as the most effective approach.

PLGA-CU Prevents Doxorubicin-Induced NF-kB Activation and Resistance

To investigate how PLGA-CU enhances breast cancer cell sensitivity to LIPO-DOXO, we examined its ability to inhibit NF-kB phosphorylation. Doxorubicin is known to activate NF-kB in breast cancer cells (Figure S5), promoting survival through downstream signaling pathways.[44] We have previously shown that immunogenic chemotherapies like doxorubicin trigger DAMPs release, which activate TLR2 signaling and lead to pro-tumoral NF-kB activation.[28] To assess whether PLGA-CU counteracts this effect, WT-874 cells were treated for 48 h with LIPO-DOXO, PLGA-CU, or the combination of both. FACS analysis revealed that LIPO-DOXO increased p-NF-kB, whereas PLGA-CU reduced it. Notably, the combination treatment completely abrogated NF-kB activation (Figure 4A). Comparable results were obtained using free CU-CPT22 and free doxorubicin. Western blot analysis confirmed that both CU-CPT22 and PLGA-CU inhibit NF-kB phosphorylation induced by doxorubicin and LIPO-DOXO in 4T1 and MDA-MB-231 cells (Figure 4B and C). Doxorubicin- and LIPO-DOXO-dependent NF-kB activation resulted in the release of the pro-tumoral cytokines IL-6 and TGF-β. This mechanism is TLR2-dependent, since the addition of CU-CPT22 and, to a greater extent, PLGA-CU significantly reduced their production to levels lower than those observed in untreated control cells (Figure 4D and E). By impairing doxorubicin-induced IL-6 production, PLGA-CU prevents CSC-dependent chemoresistance. Indeed, treatment of 4T1 cells with recombinant IL-6 stimulated CSC self-renewal, as demonstrated by the increased generation of CSC-enriched tumorspheres and increased expression of the CSC marker Sca1 (Figure 4F–H). Moreover, IL-6 treatment slightly

 https://doi.org/10.2147/IJN.S556284

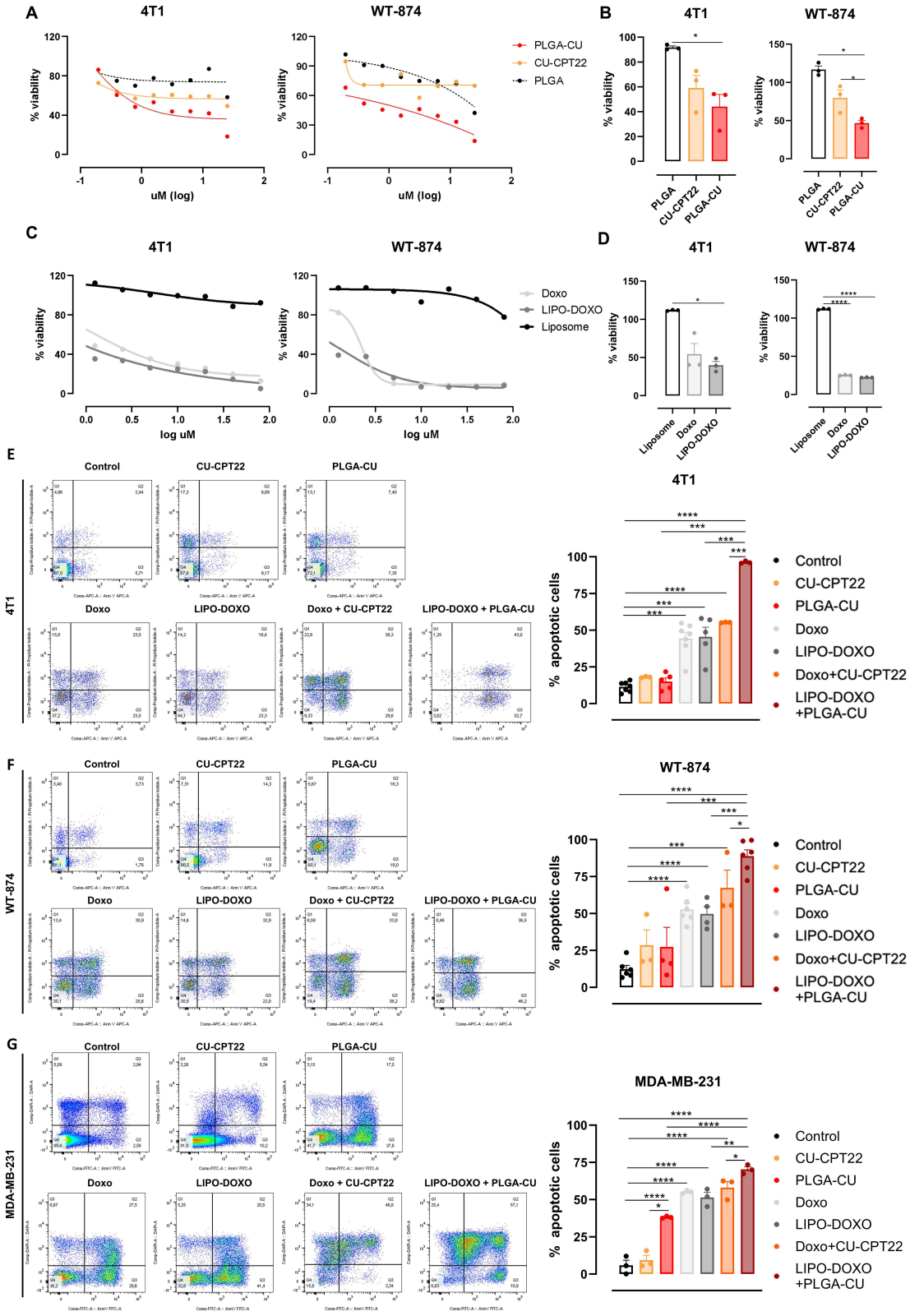

Figure 3 PLGA-CU and LIPO-DOXO impair breast cancer cell viability. MTT assays on 4T1 and WT-874 cell lines treated for 48 h with (**A**) empty PLGA, PLGA-CU or free CU-CPT22 or (**C**) empty liposome, LIPO-DOXO or free doxorubicin at various concentrations. Cell viability of the same cell lines treated with (**B**) 5 μM PLGA-CU or CU-CPT22 for 48 h with or with (**D**) 1 μM LIPO-DOXO or doxorubicin, or with empty NPs (N = 3 independent experiments). (**E**–**G**) 4T1, WT-879, and MDA-MB-231 cells were treated with PLGA-CU, LIPO-DOXO or the free drugs for 48 h and analyzed using Annexin-V/propidium iodide FACS staining. Representative density plots are shown. The graphs show individual values and means ± SEM of the % of Annexin-V^+ from 6 independent experiments. *P < 0.05, **P < 0.01; ***P < 0.001, ****P < 0.0001, One-Way ANOVA.

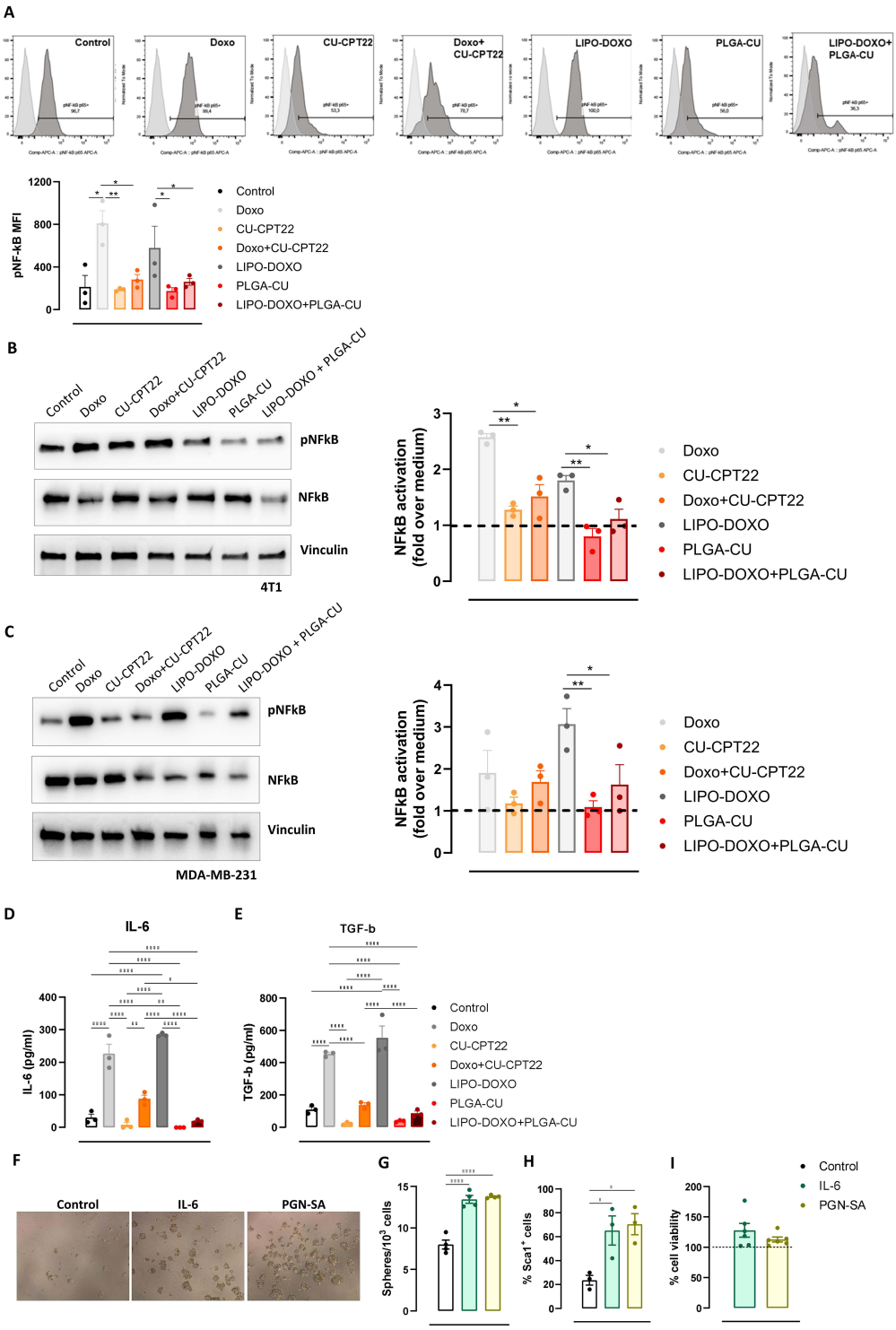

Figure 4 PLGA-CU prevents doxorubicin-induced NF-kB activation. (**A**) FACS analysis of p65 NF-κB phosphorylation in WT-874 cells treated with 5 μM CU-CPT22 or PLGA-CU and/or 1 μM LIPO-DOXO or doxorubicin for 48 h, or left untreated. The individual values and means ± SEM of mean fluorescence intensity (MFI) from three independent experiments are reported, as well as representative FACS histograms where light grey histograms show the signal obtained with an isotype control antibody, dark grey histograms with the specific monoclonal antibody. (**B** and **C**) Representative Western blot analysis of phosphorylated and total p65 NF-κB in 4T1 and MDA-MB-231 cells treated as in (**A**). The graphs report the individual values and means ± SEM of the fold increase in NF-κB phosphorylation in treated samples as compared to control cells cultured in medium from three independent experiments. The black dotted line indicates the baseline activation level of control (medium) cells. (**D** and **E**) ELISA of IL-6 and TGF-β released into the supernatant of 4T1 cells cultured for 48 h as described in (**A**). (**F** and **G**) Representative images of tumorspheres (Magnification 10X), and graph showing sphere-generating ability (number of tumorspheres generated every 10^3 plated cells) of 4T1 cells cultured for 5 days in tumorsphere-forming conditions in the absence or presence of IL-6 (10 ng/mL) or PGN-SA (200 μg/mL). (**H**) Means ± SEM of the percentage of $Sca1^+$ cells in 4T1 tumorspheres treated as in (**F**). (**I**) MTT assays on 4T1 cells treated for 48 h with IL-6 (10 ng/mL) or PGN-SA (200 μg/mL). The black dotted line represents the viability of the control condition, normalized to 100%. Deviations above or below this line indicate an increase or decrease in cell viability relative to the control. In all panels, N = 3 independent experiments. *P < 0.05, **P < 0.01, ***P < 0.001, One-way ANOVA.

https://doi.org/10.2147/IJN.S556284

enhanced 4T1 cell proliferation (Figure 4I), supporting the cancer cell intrinsic pro-tumorigenic effect of IL-6. Of note, similar results were obtained using the TLR2 ligand PGN-SA, further confirming its involvement in CSC survival and chemoresistance (Figure 4F–I).

These findings demonstrate that PLGA-CU effectively blocks doxorubicin-induced NF-kB activation and the production of pro-tumorigenic cytokines, likely restoring chemosensitivity by inhibiting TLR2-dependent CSC self-renewal and expansion.

PLGA-CU and LIPO-DOXO Accumulate in Breast Tumors

We previously demonstrated that RGD-tagged PLGAs, targeting $\alpha_v\beta_3$ integrin on cancer and endothelial cells,[45] accumulate more efficiently in tumors than their non-targeted counterparts.[23] To assess whether RGD-tagged PLGA-CU and LIPO-DOXO enhance tumor-specific drug delivery, NPs were labeled with the fluorescent probe Cy5 and Gd complexes (amphiphilic Gd-DOTAMA for PLGA-CU and hydrophilic ProHance$^{(R)}$ for LIPO-DOXO). BALB/c mice bearing orthotopic 4T1 tumors (100 mm^3) received i.p. injections of Cy5-labeled PLGA-CU or LIPO-DOXO. The i.p. systemic administration route was chosen for many advantages which are very important in preclinical studies as i) easier, faster and less invasive administration route, especially in small animals subjected to repeated high-volume dosing of drugs, ii) slower absorption in the bloodstream respect to i.v., leading to prolonged exposure to drugs, iii) potentially reduced systemic toxicity, iv) loading by the lymphatic system, supporting tumor accumulation through lymphatic transport.

Fluorescence was monitored at various time points using optical imaging. PLGA-CU showed progressive tumor accumulation, peaking at 24 h, while LIPO-DOXO peaked at 4 h and remained stable up to 24 h (Figure 5A and B). Both NPs showed minimal signal in muscle tissue, confirming tumor selectivity.

To further assess biodistribution, major organs were harvested 24 h post-injection. Both NPs accumulated in tumors, with minimal fluorescence observed in spleen, lungs, and muscle (Figure 5C). Tumor uptake was comparable between PLGA-CU and LIPO-DOXO. Liver signal was slightly elevated in PLGA-CU-treated mice, while both liver and kidney signals were observed in LIPO-DOXO-treated mice, consistent with known clearance routes of PLGAs and LIPOs.

For additional validation, Gd levels were quantified ex vivo by ICP-MS. PLGA-CU was detectable in tumors as early as 4 h post-injection and significantly increased by 24 h. In contrast, LIPO-DOXO accumulated in tumors within 4 h, with no further significant increase at 24 h (Figure 5D).

These results confirm that both PLGA-CU and LIPO-DOXO selectively accumulate in breast tumors. To assess their in vivo anti-cancer efficacy, preliminary dose-finding experiments were performed. BALB/c mice bearing 4T1 tumors were treated with i.p. injections of vehicle, untargeted PLGA-CU, or RGD-targeted PLGA-CU (2.5 or 5 mg/kg CU-CPT22), administered four times. Only RGD-PLGA-CU significantly reduced tumor growth, with the 5 mg/kg dose being more effective (Figure 5E and F), confirming its anti-tumor activity in vivo.

This is due to the enhanced accumulation of RGD-targeted PLGA-CU in tumors as compared to untargeted ones, as demonstrated by the quantification of Gd levels by ICP-MS after 24 h (Figure 5G). To determine whether RGD functionalization also enhances LIPO-DOXO anti-cancer efficacy, 4T1-tumor bearing mice were treated with either untargeted or RGD-targeted LIPO-DOXO (3 mg/kg doxorubicin). While untargeted LIPO-DOXO had no significant effect, RGD-targeted LIPO-DOXO markedly reduced tumor growth (Figure 5H). The efficacy of RGD-LIPO-DOXO was further confirmed in HER2/neu transgenic BALB-neuT mice, where it significantly inhibited spontaneous mammary tumor growth, an effect not observed with free doxorubicin (Figure 5I).

PLGA-CU Improves the Anti-Cancer Efficacy of LIPO-DOXO in vivo

To evaluate the combined therapeutic efficacy of PLGA-CU and LIPO-DOXO, BALB/c mice bearing 4T1 tumors were randomized into four groups: vehicle, PLGA-CU (5 mg/kg), LIPO-DOXO (3 mg/kg doxorubicin), or combination of PLGA-CU and LIPO-DOXO. Treatments were administered i.p. twice weekly for a total of four doses. Administration of PLGA-CU and LIPO-DOXO, alone or in combination, did not induce systemic toxicity, as demonstrated by the lack of reduction of body weight in treated mice as compared to the controls (Figure 6A). Moreover, the treatments did not induce any detectable alterations in posture or locomotor activity, nor did they result in changes in coat appearance,

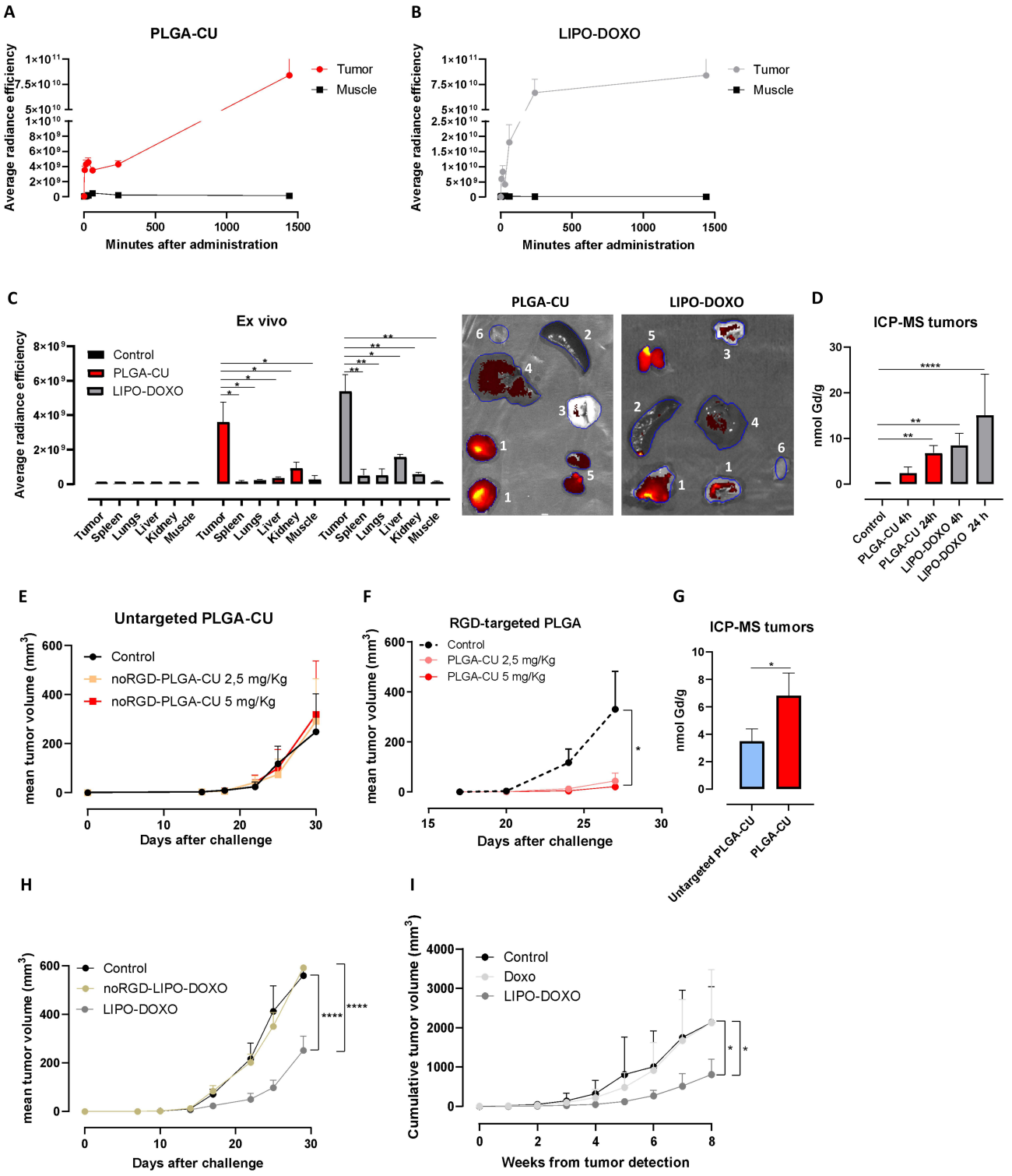

Figure 5 RGD improves the accumulation of the NPs in tumors and is necessary for their in vivo efficacy. (**A**–**C**) In vivo and ex vivo optical imaging of 4T1 tumor-bearing mice. 4T1 tumor-bearing mice were injected i.p. with Cy5-containing PLGA-CU and LIPO-DOXO (1 nmol Cy5/mouse; N = 6 per group). (**A** and **B**) Tumor and muscle accumulation (average radiance efficiency) in function of time. (**C**) Ex vivo biodistribution in organs dissected 24 h after injection (N = 3 mice per group). The graph shows the mean ± SEM of average radiance efficiency in the different organs. Representative optical imaging of tumors (1), spleens (2), lungs (3), livers (4), kidneys (5) and muscles (6) from PLGA-CU and LIPO-DOXO-injected mice. Images are normalized to the same color scale. (**D**) ICP-MS quantification of Gd retained in the tumors of mice injected with Gd-containing PLGA-CU or LIPO-DOXO at 4 or 24 h. (**E**–**H**) BALB/c mice were orthotopically challenged with 4T1 cells. When the tumors reached 2 mm in diameter, mice were treated i.p. with vehicle or with (**E**) untargeted PLGA-CU, (**F**) RGD-targeted PLGA-CU (2.5 or 5 mg/kg) or (**H**) untargeted or RGD-targeted LIPO-DOXO (3 mg/kg). The treatment was repeated twice per week for a total of 5 administrations. Graphs show mean tumor volumes (N = 6 mice per group). (**G**) ICP-MS quantification of Gd retained in the tumors of mice injected with RGD-targeted or untargeted Gd-containing PLGA-CU at 24 h. (**I**) 15–17 weeks old BALB-neuT mice were treated once per week with either doxorubicin (2 mg/kg), LIPO-DOXO (2 mg/kg) or vehicle for a total of seven weeks, starting when the first tumor became palpable. The graph shows the mean cumulative tumor volume of all tumors of a mouse (N = 10 mice per group). *P < 0.05; **P < 0.01, ****P < 0.0001; One-Way (**A**–**D**) or Two-Way (**E**–**H**) ANOVA.

https://doi.org/10.2147/IJN.S556284

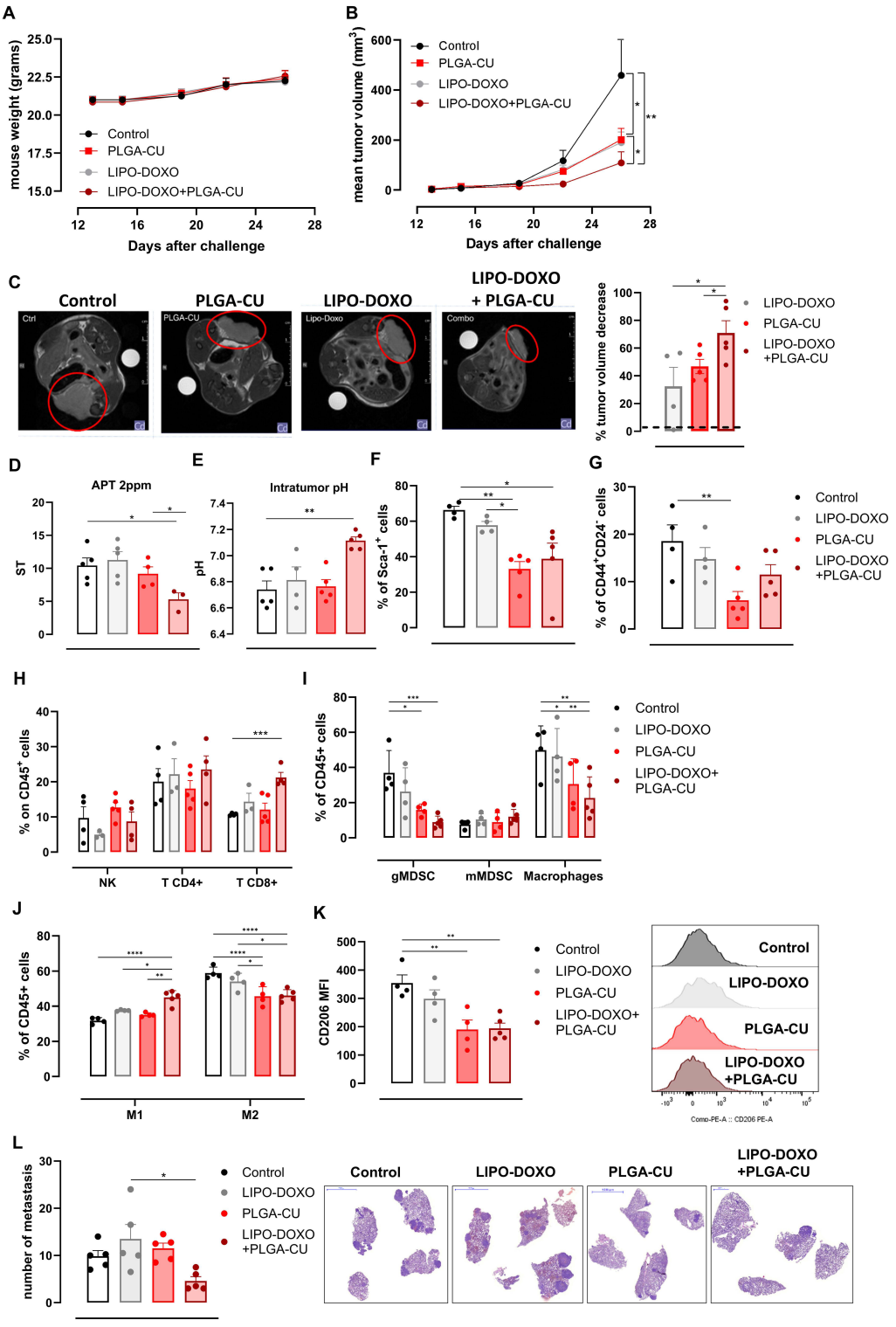

Figure 6 PLGA-CU enhances the anti-tumor effects of LIPO-DOXO. 4T1-tumor bearing mice were treated i.p. with vehicle or RGD-targeted PLGA-CU (5 mg/kg) or LIPO-DOXO (3 mg/kg) (N = 5 mice per group). The treatment was repeated twice per week for a total of 4 administrations. (**A**) The graph shows mean ± SEM of the mouse body weight. (**B**) The graph shows mean ± SEM of the tumor volume. (**C**) Representative T2w axial MR images acquired at the endpoint of control and treated mice. Tumor volume was measured by manually drawing ROIs in the tumor for all axial slices covering the entire tumor (Fiji-ImageJ free software). The graph reports single values and means ± SEM of the percentage of tumor volume decrease in treated mice as compared to control mice (N = 5 per group). (**D**) CEST-MRI analysis of the intratumor 2 ppm peak associated with creatine levels and (**E**) intratumor pH measurement through the AACID CEST-MRI sequence (N = 5 per group). FACS analysis of (**F**) Sca1$^+$ and (**G**) CD44$^+$CD24$^-$ CSCs among CD45$^-$ cells, and (**H**) CD8$^+$ T cells, CD4$^+$ T cells, and NK cells, (**I**) Ly6G$^+$ granulocytic MDSCs, Ly6C$^+$ monocytic MDSCs and macrophages among CD45$^+$ cells. (**J**) FACS analysis of MHC II$^+$ M1 and CD206$^+$ M2 polarized macrophages among the macrophage population in the tumors. Graphs show individual values and means ± SEM of the percentage of positive cells in the different mice (N ≥ 4 per group). (**K**) The graph shows individual values and means ± SEM of the CD206 MFI in intratumoral macrophages (N ≥ 4 per group). Representative FACS histograms are shown. (**L**) Means ± SEM of the number of spontaneous lung metastases. Each circle represents a mouse (N = 5 per group). Representative H&E images of metastatic lungs are shown (scale bars in blue). *P < 0.05; **P < 0.01, ****P < 0.0001; One-Way or Two-Way (**A** and **B**) ANOVA.

grooming behavior, or food and water intake, nor in the induction of piloerection, hypo-/hyperactivity, tremors, hunched posture, porphyrin staining, dehydration, or respiratory irregularities (not shown). Collectively, these findings indicate that the administered treatments do not elicit systemic toxicity in mice. Both monotherapies significantly inhibited tumor growth, but their combination nearly halted tumor progression (Figure 6B). MRI confirmed a reduction in tumor volume in all treated groups, with the combination therapy achieving a 71% reduction (Figure 6C). To further assess treatment effects, CEST-MRI was performed prior to sacrifice. Tumors from the combination group showed a marked decrease in the $CEST_{@2ppm}$ signal compared to controls and LIPO-DOXO-treated groups (Figure 6D). The $CEST_{@2ppm}$ correlates creatine levels.[37,38] Herein, we show that $CEST_{@2ppm}$ is reduced in tumor of mice treated with the combination of LIPO-DOXO and PLGA-CU, suggesting that the treatment reduces creatine level in the tumor. While creatine was historically considered tumor-suppressive, recent evidence supports its pro-tumoral and pro-metastatic roles.[38,46]

Because the $CEST_{@2ppm}$ signal is also influenced by pH, we employed the AACID (Amine and Amide Concentration Independent Detection) CEST-MRI sequence[39] for non-invasive tumor pH measurement. Mice treated with vehicles, PLGA-CU, or LIPO-DOXO showed similarly acidic tumor pH values (pH 6.7–6.9), with no significant differences. In contrast, tumors from mice receiving the combination of LIPO-DOXO + PLGA-CU exhibited a partial pH normalization, reaching pH 7.1±0.1 (Figure 6E), indicating an improved TME.

As TLR2 promotes CSC self-renewal, and CSCs drive tumor progression and resistance, we analyzed CSC populations in excised tumors by FACS analysis. PLGA-CU significantly reduced Sca1+ and CD44+CD24− CSC populations, an effect that was also evident in the combination group (Figure 6F and G).

Beyond its direct effects on cancer cells, TLR2 inhibition can also modulate the immune microenvironment through several mechanisms, including the release of immunosuppressive cytokines such as IL-6 and TGF-β. Accordingly, the combination treatment increased intratumor $CD8^+$ T cell infiltration (Figure 6H).

Moreover, PLGA-CU, alone or combined with LIPO-DOXO, induced a significant reduction in $Ly6G^+$ granulocytic MDSCs and tumor associated macrophages, while no significant modulation of $Ly6C^+$ monocytic MDSCs were observed (Figure 6I). Moreover, the combined therapy significantly increased anti-tumor M1 while decreasing immunosuppressive M2 macrophages, and the expression levels of their marker CD206 (Figure 6J and K). These data demonstrate that TLR2 blockade reverses breast cancer-associated immunosuppression. Importantly, the combination treatment significantly reduced the number of lung metastases (Figure 6L), highlighting its potent anti-metastatic activity and overall therapeutic benefit.

PLGA-CU Reduces Tumor Angiogenesis

The role of TLR2 in cancer extends beyond tumor and immune cells, affecting other components of the TME, particularly the vasculature. TLR2 is expressed by endothelial cells and can be activated by TME-derived ligands, potentially driving angiogenesis and tumor progression.[47] Additionally, TLR2 activation in cancer cells enhances angiogenesis by stimulating the release of pro-angiogenic cytokines such as VEGF.[8]

To evaluate the impact of TLR2 inhibition on tumor vasculature, we performed IHC analysis of CD31 in tumors from treated and control mice. PLGA-CU, both alone and in combination with LIPO-DOXO, significantly reduced vascular density compared to untreated or LIPO-DOXO-treated tumors (Figure 7A and B). To elucidate the underlying mechanism, VEGF secretion was measured in both breast cancer and tumor endothelial cells after 48 h of treatment with free or NP-formulated drugs. In 4T1 cells, LIPO-DOXO and free doxorubicin increased VEGF secretion, an effect suppressed by CU-CPT22 and PLGA-CU, even when combined with doxorubicin or LIPO-DOXO (Figure 7C). Similar results were observed in human MDA-MB-231 TNBC cells and murine bEnd.3 endothelial cells (Figure 7D and E), confirming that TLR2-dependent VEGF regulation occurs in both tumor and endothelial compartments.

Beyond promoting VEGF production, TLR2 appears to protect endothelial cells from chemotherapy-induced apoptosis. Free doxorubicin and LIPO-DOXO induced minimal apoptosis in bEnd.3 cells, suggesting an intrinsic resistance. CU-CPT22 alone had no significant effect, while PLGA-CU moderately increased apoptosis. Notably, combining CU-CPT22 with free doxorubicin, or PLGA-CU with LIPO-DOXO, significantly enhanced endothelial cell apoptosis compared to single treatments, indicating that TLR2 inhibition sensitizes tumor endothelial cells to chemotherapy (Figure 7F).

 https://doi.org/10.2147/IJN.S556284

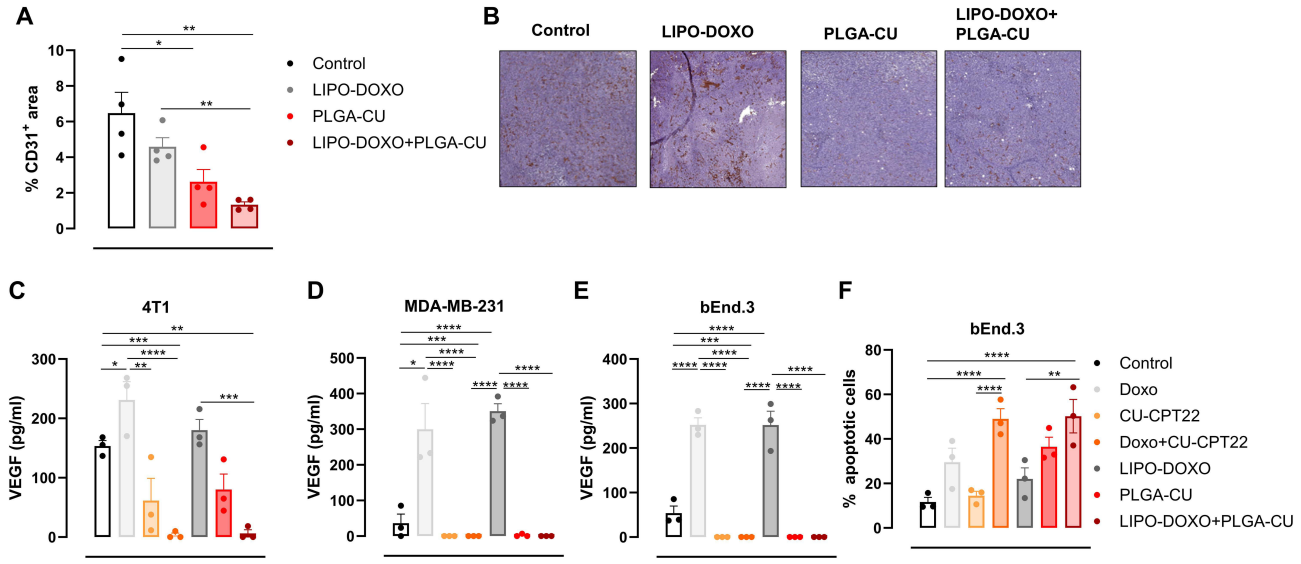

Figure 7 PLGA-CU impairs angiogenesis. (**A**) Individual values and means ± SEM of the % of $CD31^+$ cells and (**B**) representative CD31 IHC staining of tumors. Magnification X20. (**C**–**E**) ELISA analysis of VEGF released into the supernatant by 4T1, MDA-MB-231 or Bend.3 cells treated with PLGA-CU and/or LIPO-DOXO or free CU-CPT22 or doxorubicin for 48 h or left untreated. The graphs show individual values and means ± SEM of VEGF concentration from three independent experiments. (**F**) bEnd.3 cells were treated as in E, then apoptosis was analyzed. The graph shows individual values and means ± SEM of the % of Annexin-V^+ from three independent experiments. *P < 0.05, **P < 0.01; ***P < 0.001, ****P < 0.0001, Two-Way (**A**) or One-Way ANOVA.

Collectively, these results highlight a pro-angiogenic role of TLR2 in breast cancer and demonstrate that its inhibition, particularly when combined with chemotherapy, disrupts tumor angiogenesis, contributing significantly to overall therapeutic efficacy.

Discussion

Despite decades of advances in cancer therapy, systemic chemotherapy continues to face significant limitations in efficacy, primarily due to therapy resistance. Both tumor intrinsic and acquired resistance mechanisms contribute to treatment failure.[3] Among these mechanisms, CSCs play a crucial role, exhibiting phenotypic plasticity, epithelial-to-mesenchymal transitions, metabolic reprogramming, and the capability to promote an immunosuppressive TME, all of which enhance chemoresistance.[48] Consequently, therapies able of targeting CSCs while simultaneously remodeling the TME to a less tumor-promoting state may significantly improve the efficacy of chemotherapy.

In addition, chemotherapy is associated with safety concerns stemming from poor tumor selectivity, off-target toxicity, and biological barriers that hinder adequate drug accumulation in the tumor. To address these challenges, nanomedicine has emerged as a promising platform, offering improved pharmacokinetics, enhanced tumor-targeting capabilities, and the potential for integration with diagnostic imaging.[49]

To overcome these chemotherapy drawbacks, we investigated a nanotheranostic strategy that combines chemotherapy with targeted therapy to eradicate CSCs and modulate the immune response. We utilized tumor-targeted liposomes and hybrid PLGA/lipid NPs loaded with doxorubicin and the TLR2 inhibitor CU-CPT22, respectively. Our previous work demonstrated that TLR2 is overexpressed in breast CSCs and plays a pivotal role in their self-renewal.[8] Therefore, the rationale for targeting TLR2 lies in its multifaceted contributions to tumor progression. TLR2 activation in cancer cells triggers the MyD88/NF-κB and AKT pathways, promoting the secretion of cytokines and growth factors, including TGF-β, VEGF, and IL-6.[8] These factors support CSC survival, self-renewal, and invasion through autocrine activation of the STAT3 and Smad3 pathways.[8] These cytokines promote CSC survival, self-renewal and invasion via the autocrine activation of the STAT3 and Smad3 pathways.[8,50,51] Moreover, NF-κB signaling drives inflammation and resistance to immunogenic chemotherapies such as doxorubicin.[6] TLR2 also fosters an immunosuppressive TME by limiting cytotoxic T cell infiltration.[52]

While CU-CPT22 has shown promising anti-cancer effects in vitro,[53] its poor aqueous solubility and untested systemic safety profile pose translational challenges. Encapsulation in hybrid PLGA/lipid NPs improved its solubility and bioavailability, enabling safe and effective systemic delivery, as demonstrated by our in vivo experiments. Biodistribution analysis confirmed tumor-specific accumulation of both PLGA-CU and LIPO-DOXO decorated with the RGD peptide, with minimal signal in non-target tissues, such as spleen, lung, and muscle, underscoring the targeted nature of our delivery systems. We have previously demonstrated that HER2-positive and TNBC cells, as well as tumor vasculature, express $\alpha_v\beta_3$ integrin,[45] which is an optimal target for drug delivery. Consistently with this, untargeted NPs failed to show anticancer activity, whereas PLGA-CU effectively counteracted doxorubicin-induced NF-κB activation and sensitized cancer cells to chemotherapy. Importantly, NP formulation preserved the biological activity of the free drug while enhancing tumor accumulation and delivery specificity. The combination of PLGA-CU and LIPO-DOXO significantly reduced triple negative breast tumor growth and the frequency of $Sca1^+$ and $CD44^+CD24^-$ CSCs. One of the major findings of this study is that TLR2 inhibition exerts therapeutic effects across multiple tumor compartments, making it a particularly attractive target. In addition to directly modulating tumor cell behavior, TLR2 inhibition also influenced TME. Notably, while treatment with LIPO-DOXO alone did not significantly alter the composition of tumor-infiltrating immune cells, its combination with PLGA-CU led to a significant increase in $CD8^+$ cytotoxic T cells, while decreasing the immunosuppressive populations. These findings suggest that TLR2 activation may facilitate tumor growth by sustaining immune suppression, in part through the release of pro-tumoral cytokines such as IL-6 and TGF-β, thereby limiting doxorubicin's ability to trigger an effective anti-tumor immune response. However, co-treatment with TLR2 inhibitors appears to unmask the immunostimulatory potential of doxorubicin-induced immunogenic cell death. Interestingly, similar outcomes were observed upon blocking HMGB1, a known TLR2 ligand, which enhanced the response to immune checkpoint inhibitors in the 4T1 model.[54] This is consistent with our previous findings demonstrating that TLR2 promotes immune evasion mechanisms,[6] and aligns with several reports indicating that the activation of TLR2 can drive the expansion of Tregs[12,55] and immunosuppressive myeloid cell populations.[50]

Furthermore, we demonstrate for the first time that CU-CPT22 reduces tumor vascularization, a critical process for tumor maintenance and metastasis. Histological analysis of tumor sections revealed a marked decrease in $CD31^+$ endothelial cells in tumors treated with PLGA-CU, alone or in combination with LIPO-DOXO, compared to controls. Since TLR2 is expressed by endothelial cells, and its activation directly promotes angiogenesis,[48] this finding underscores the relevance of TLR2 as a vascular target. Treatment of tumor endothelial cells with PLGA-CU, particularly in combination with LIPO-DOXO, significantly induced apoptosis. This was accompanied by a reduction in VEGF levels produced by both cancer and endothelial cells, suggesting that TLR2 inhibition impairs angiogenesis through both direct effects on endothelial cells and indirect effects via VEGF modulation.

Interestingly, CEST-MRI analysis revealed altered tumor metabolism upon treatment, particularly a reduction in creatine levels following combination therapy. While the precise role of creatine in tumor progression remains debated, recent studies suggest that it may have context-dependent pro- or anti-tumoral effects.[46] Specifically, high levels of creatine in fasting plasma are associated with increased risk of developing breast cancer,[56] and upregulation of genes involved in creatine biosynthesis or uptake has been linked to breast cancer progression and poor prognosis.[57] Moreover, it has been shown that adipocytes produce high levels of creatine, which can be utilized by neighboring breast cancer cells to generate ATP and support proliferation.[50] Therefore, the observed decrease in creatine content in tumors treated with PLGA-CU and LIPO-DOXO correlates with reduced tumor growth. However, it remains unclear whether this reduction in creatine is a direct result of altered cancer metabolism induced by the therapy or a secondary effect of effective tumor targeting. Additionally, the combination treatment restored intratumoral pH. As extensively reported in literature, solid tumors, particularly the aggressive ones, often exhibit an acidic microenvironment. Here, the combined therapy counteracts this trend, suggesting a favorable therapeutic response, although the underlying mechanisms need to be further elucidated.

Conclusions

In conclusion, our study provides compelling evidence that TLR2 is a central regulatory node in tumor biology, influencing cancer cell proliferation, immune modulation, and vascular remodeling. These findings position TLR2 as

a strategic therapeutic target in breast cancer. By developing PLGA NPs encapsulating the TLR2 inhibitor CU-CPT22 and liposomes loaded with doxorubicin, we demonstrate that coordinated inhibition of TLR2 signaling and administration of chemotherapy effectively impair tumor progression. Results support the feasibility of TLR2-targeted nanotheranostic strategies as a promising approach for solid tumor treatment and underscore the therapeutic potential of multicompartmental targeting to overcome key barriers, including stromal remodeling and immunosuppressive signaling, that contribute to therapy resistance in breast cancer.

Importantly, the safety profile observed in our in vivo experiments suggests that the proposed nanoformulations do not induce systemic toxicity, as evidenced by stable body-weight curves and the absence of clinical signs of distress or behavioral alterations throughout the study. Nevertheless, some limitations should be acknowledged. First, an extended histopathological evaluation of liver, kidney, and heart tissues was not performed. Although the physiological and behavioral monitoring of the animals did not reveal indications of systemic side effects, a more comprehensive organ-specific toxicological assessment will be necessary to fully define the safety profile of these formulations. Second, drug administration was performed i.p. rather than i.v. while i.p. delivery is widely used in preclinical studies for practical and ethical reasons, translation to a clinical setting will require optimization of i.v. formulations to ensure appropriate pharmacokinetics, biodistribution, and compatibility with standard oncological delivery routes.

Taken together, our work provides proof-of-concept for a dual-targeting nanotherapeutic strategy aimed at modulating tumor-cell intrinsic pathways and the TME. Future studies addressing pharmacokinetics, systemic toxicity, and i.v. delivery will be essential to advance these nanoformulations toward clinical translation. Despite these limitations, the present findings lay the groundwork for innovative TLR2-focused nanomedicines and highlight the broader potential of rational combinatorial targeting for the treatment of solid tumors.

Abbreviations

APT, amide proton transfer; ANOVA, analysis of variance; BCA, bicinchoninic acid; Breg, Regulatory B cell; CEST, chemical exchange saturation transfer; CSC, cancer stem cell; DLS, dynamic light scattering; DWI, diffusion-weighted imaging; ECL, enhanced chemiluminescence; ELISA, enzyme-linked immunosorbent assay; FACS, fluorescence-activated cell sorting; FOV, field of view; gadolinium: Gd Gd-DOTAMA, gadolinium(III)-1,4,7,10-tetraazacyclododecane-1,4,7,10-tetra(methylenephosphonic acid); HER2, human epidermal growth factor receptor 2; HMGB1, high mobility group box 1; HPLC, high-performance liquid chromatography; ICP-MS, inductively coupled plasma mass spectrometry; IHC, immunohistochemistry; IL, interleukin; i.p., intraperitoneal; LIPO, liposome; MFI, mean fluorescence intensity; MRI, magnetic resonance imaging; MS, mass spectrometry; MTT, 3-(4,5-dimethylthiazol-2-yl)-2,5-diphenyltetrazolium bromide; NF-κB, nuclear factor kappa-light-chain-enhancer of activated B cells; NMR, nuclear magnetic resonance; NP, nanoparticles; PBS, phosphate-buffered saline; PCR, polymerase chain reaction; PEG, polyethylene glycol; PLGA, poly(lactic-co-glycolic acid); RGD, arginine-glycine-aspartic acid; ROI, region of interest; SDS-PAGE, sodium dodecyl sulfate-polyacrylamide gel electrophoresis; SEM, standard error of the mean; TGF-β, tumor growth factor β; TLR2, toll-like receptor 2; TME, tumor microenvironment; TNBC, triple-negative breast cancer; Tregs, regulatory T cells; TSP, trimethylsilylpropanoic acid; UV/Vis, ultraviolet-visible spectroscopy; VEGF, vascular endothelial growth factor.

Data Sharing Statement

All data analyzed during this study are included in this published article.

Ethics Approval

Animal studies were approved by the Animal Care and Use Committee of the University of Turin and the Italian Ministry of Health (authorization N° 10/2023-PR; CC652.191, CC652.191.EXT.74 and 469/2021-PR; CC652.154).

Acknowledgment

This paper is partly based on the thesis of Dr. Antonino Di Lorenzo. It has been published on the institutional website: https://iris.unito.it/handle/2318/2064164?mode=full. Antonino Di Lorenzo and Chiara Romiti share first autorship.

Author Contributions

All authors made a significant contribution to the work reported, whether that is in the conception, study design, execution, acquisition of data, analysis and interpretation, or in all these areas; took part in drafting, revising or critically reviewing the article; gave final approval of the version to be published; have agreed on the journal to which the article has been submitted; and agree to be accountable for all aspects of the work. Antonino Di Lorenzo and Chiara Romiti share first autorship. Enza Di Gregorio and Laura Conti share last and corresponding authorship.

Funding

The research leading to these results has received funding from AIRC [IG 2021 – ID. 25766 project]- principal investigator L. Conti, from the University of Turin, from the Fondazione Cassa di Risparmio di Torino (CRT) (G. Ferrauto) and from Progetti di Rilevante Interesse Nazionale-PRIN [2022TRSH52] (C. Curcio) and [20222HY5TF] (G. Ferrauto).The Italian Ministry for University and Research (MUR) is gratefully acknowledged for yearly FOE funding to the Euro-BioImaging Multi-Modal Molecular Imaging Italian Node (MMMI).

Disclosure

The authors report no conflicts of interest in this work.

References

1. Tarantino P, Tolaney SM. Progress in breast cancer management. *Lancet*. 2024;404(10461):1376–1378. doi:10.1016/S0140-6736(24)01823-3
2. Siegel RL, Kratzer TB, Giaquinto AN, Sung H, Jemal A. Cancer statistics, 2025. *CA Cancer J Clin*. 2025;75(1):10–45. doi:10.3322/caac.21871
3. Lukasiewicz S, Czeczelewski M, Forma A, Baj J, Sitarz R, Stanislawek A. Breast cancer-epidemiology, risk factors, classification, prognostic markers, and current treatment strategies-an updated review. *Cancers*. 2021;13(17). doi:10.3390/cancers13174287
4. Ji X, Lu Y, Tian H, Meng X, Wei M, Cho WC. Chemoresistance mechanisms of breast cancer and their countermeasures. *Biomed Pharmacother*. 2019;114:108800. doi:10.1016/j.biopha.2019.108800
5. Meng LN, Zheng Y, Liu H, Fan DM. The tumor microenvironment: a key player in multidrug resistance in cancer. *Oncologie*. 2024;26(1):41–58. doi:10.1515/oncologie-2023-0459
6. Di Lorenzo A, Bolli E, Ruiu R, et al. Toll-like receptor 2 promotes breast cancer progression and resistance to chemotherapy. *Oncoimmunology*. 2022;11(1):2086752. doi:10.1080/2162402X.2022.2086752
7. Wang Y, Liu S, Zhang Y, Yang J. Dysregulation of TLR2 serves as a prognostic biomarker in breast cancer and predicts resistance to endocrine therapy in the luminal B subtype. *Front Oncol*. 2020;10:547. doi:10.3389/fonc.2020.00547
8. Conti L, Lanzardo S, Arigoni M, et al. The noninflammatory role of high mobility group box 1/Toll-like receptor 2 axis in the self-renewal of mammary cancer stem cells. *FASEB J*. 2013;27(12):4731–4744. doi:10.1096/fj.13-230201
9. Sutmuller RP, den Brok MH, Kramer M, et al. Toll-like receptor 2 controls expansion and function of regulatory T cells. *J Clin Invest*. 2006;116(2):485–494. doi:10.1172/JCI25439
10. McBride A, Konowich J, Salgame P. Host defense and recruitment of Foxp3(+) T regulatory cells to the lungs in chronic Mycobacterium tuberculosis infection requires toll-like receptor 2. *PLoS Pathog*. 2013;9(6):e1003397. doi:10.1371/journal.ppat.1003397
11. Tang M, Diao J, Gu H, Khatri I, Zhao J, Cattral MS. Toll-like receptor 2 activation promotes tumor dendritic cell dysfunction by regulating IL-6 and IL-10 receptor signaling. *Cell Rep*. 2015;13(12):2851–2864. doi:10.1016/j.celrep.2015.11.053
12. Chen YQ, Li PC, Pan N, et al. Tumor-released autophagosomes induces CD4(+) T cell-mediated immunosuppression via a TLR2-IL-6 cascade. *J Immunother Cancer*. 2019;7(1):178. doi:10.1186/s40425-019-0646-5
13. Ye L, Zhang Q, Cheng Y, et al. Tumor-derived exosomal HMGB1 fosters hepatocellular carcinoma immune evasion by promoting TIM-1(+) regulatory B cell expansion. *J Immunother Cancer*. 2018;6(1):145. doi:10.1186/s40425-018-0451-6
14. Kim S, Takahashi H, Lin WW, et al. Carcinoma-produced factors activate myeloid cells through TLR2 to stimulate metastasis. *Nature*. 2009;457(7225):102–106. doi:10.1038/nature07623
15. Sinha P, Clements VK, Bunt SK, Albelda SM, Ostrand-Rosenberg S. Cross-talk between myeloid-derived suppressor cells and macrophages subverts tumor immunity toward a type 2 response. *J Immunol*. 2007;179(2):977–983. doi:10.4049/jimmunol.179.2.977
16. Lundy J, Gearing LJ, Gao H, et al. TLR2 activation promotes tumour growth and associates with patient survival and chemotherapy response in pancreatic ductal adenocarcinoma. *Oncogene*. 2021;40(41):6007–6022. doi:10.1038/s41388-021-01992-2
17. Zhang W, Liu W, Hu X. Robinin inhibits pancreatic cancer cell proliferation, EMT and inflammation via regulating TLR2-PI3k-AKT signaling pathway. *Cancer Cell Int*. 2023;23(1):328. doi:10.1186/s12935-023-03167-3
18. Farnebo L, Shahangian A, Lee Y, Shin JH, Scheeren FA, Sunwoo JB. Targeting Toll-like receptor 2 inhibits growth of head and neck squamous cell carcinoma. *Oncotarget*. 2015;6(12):9897–9907. doi:10.18632/oncotarget.3393
19. Grabowski M, Murgueitio MS, Bermudez M, Wolber G, Weindl G. The novel small-molecule antagonist MMG-11 preferentially inhibits TLR2/1 signaling. *Biochem Pharmacol*. 2020;171:113687. doi:10.1016/j.bcp.2019.113687
20. Gavas S, Quazi S, Karpinski TM. Nanoparticles for cancer therapy: current progress and challenges. *Nanoscale Res Lett*. 2021;16(1):173. doi:10.1186/s11671-021-03628-6
21. Alessandro Amaolo HS, Carrera C, Padovan S, Carniato F, Di Gregorio E, Ferrauto G. Cellular uptake of hybrid PLGA-lipid gadolinium nanoparticles functionalized for magnetic resonance imaging of pancreatic adenocarcinoma cells. *ACS Nanoscience Au*. 2025;5(3):184–195. doi:10.1021/acsnanoscienceau.5c00010

22. Ding D, Zhu Q. Recent advances of PLGA micro/nanoparticles for the delivery of biomacromolecular therapeutics. *Mater Sci Eng C Mater Biol Appl*. 2018;92:1041–1060. doi:10.1016/j.msec.2017.12.036
23. Vanni S, Caputo TM, Cusano AM, et al. Engineered anti-HER2 drug delivery nanosystems for the treatment of breast cancer. *Nanoscale*. 2025;17 (15):9436–9457. doi:10.1039/d4nr03907f
24. Sakhi M, Khan A, Iqbal Z, et al. Design and characterization of paclitaxel-loaded polymeric nanoparticles decorated with trastuzumab for the effective treatment of breast cancer. *Front Pharmacol*. 2022;13:855294. doi:10.3389/fphar.2022.855294
25. Grange C, Geninatti-Crich S, Esposito G, et al. Combined delivery and magnetic resonance imaging of neural cell adhesion molecule-targeted doxorubicin-containing liposomes in experimentally induced Kaposi's sarcoma. *Cancer Res*. 2010;70(6):2180–2190. doi:10.1158/0008-5472.CAN-09-2821
26. Ferrauto G, Tripepi M, Di Gregorio E, Bitonto V, Aime S, Delli Castelli D. Detection of U-87 tumor cells by RGD-functionalized/Gd-containing giant unilamellar vesicles in magnetization transfer contrast magnetic resonance images. *Invest Radiol*. 2021;56(5):301–312. doi:10.1097/RLI.0000000000000742
27. Lanzardo S, Conti L, Brioschi C, et al. A new optical imaging probe targeting alphaVbeta3 integrin in glioblastoma xenografts. *Contrast Media Mol Imaging*. 2011;6(6):449–458. doi:10.1002/cmmi.444
28. Di Gregorio E, Romiti C, Di Lorenzo A, Cavallo F, Ferrauto G, Conti L. RGD_PLGA nanoparticles with docetaxel: a route for improving drug efficiency and reducing toxicity in breast cancer treatment. *Cancers*. 2022;15(1):8. doi:10.3390/cancers15010008
29. Di Gregorio E, Lattuada L, Maiocchi A, Aime S, Ferrauto G, Gianolio E. Supramolecular adducts between macrocyclic Gd(iii) complexes and polyaromatic systems: a route to enhance the relaxivity through the formation of hydrophobic interactions. *Chem Sci*. 2020;12(4):1368–1377. doi:10.1039/d0sc03504a
30. Anelli PL, Lattuada L, Lorusso V, Schneider M, Tournier H, Uggeri F. Mixed micelles containing lipophilic gadolinium complexes as MRA contrast agents. *MAGMA*. 2001;12(2–3):114–120. doi:10.1007/BF02668092
31. Barge A, Cravotto G, Gianolio E, Fedeli F. How to determine free Gd and free ligand in solution of Gd chelates. A technical note. *Contrast Media Mol Imaging*. 2006;1(5):184–188. doi:10.1002/cmmi.110
32. Abraham SA, Waterhouse DN, Mayer LD, Cullis PR, Madden TD, Bally MB. The liposomal formulation of doxorubicin. *Methods Enzymol*. 2005;391:71–97. doi:10.1016/S0076-6879(05)91004-5
33. Conti L, Bolli E, Di Lorenzo A, et al. Immunotargeting of the xCT cystine/glutamate antiporter potentiates the efficacy of HER2-targeted immunotherapies in breast cancer. *Cancer Immunol Res*. 2020;8(8):1039–1053. doi:10.1158/2326-6066.CIR-20-0082
34. Rolih V, Caldeira J, Bolli E, et al. Development of a VLP-based vaccine displaying an xCT extracellular domain for the treatment of metastatic breast cancer. *Cancers*. 2020;12(6):1492. doi:10.3390/cancers12061492
35. Boggio K, Nicoletti G, Di Carlo E, et al. Interleukin 12-mediated prevention of spontaneous mammary adenocarcinomas in two lines of Her-2/neu transgenic mice. *J Exp Med*. 1998;188(3):589–596. doi:10.1084/jem.188.3.589
36. Curcio C, Mucciolo G, Roux C, et al. PI3Kgamma inhibition combined with DNA vaccination unleashes a B-cell-dependent antitumor immunity that hampers pancreatic cancer. *J Exp Clin Cancer Res*. 2024;43(1):157. doi:10.1186/s13046-024-03080-1
37. Di Gregorio E, Papi C, Conti L, et al. A magnetic resonance imaging-chemical exchange saturation transfer (MRI-CEST) method for the detection of water cycling across cellular membranes. *Angew Chem Int Ed Engl*. 2024;63(6):e202313485. doi:10.1002/anie.202313485
38. Cai K, Singh A, Poptani H, et al. CEST signal at 2ppm (CEST@2ppm) from Z-spectral fitting correlates with creatine distribution in brain tumor. *NMR Biomed*. 2015;28(1):1–8. doi:10.1002/nbm.3216
39. Albatany M, Meakin S, Bartha R. Brain pH measurement using AACID CEST MRI incorporating the 2 ppm amine resonance. *Tomography*. 2022;8 (2):730–739. doi:10.3390/tomography8020060
40. Di Gregorio E, Ferrauto G, Furlan C, et al. The issue of gadolinium retained in tissues: insights on the role of metal complex stability by comparing metal uptake in murine tissues upon the concomitant administration of lanthanum- and gadolinium-diethylentriamminopentaacetate. *Invest Radiol*. 2018;53(3):167–172. doi:10.1097/RLI.0000000000000423
41. Edel Sah HS, Sowrirajan H, Persaud I, Podila R, Brown JM. Recent trends in preparation of Poly(lactide-co-glycolide) nanoparticles by mixing polymeric organic solution with antisolvent. *J Nanomater*. 2015;2015. doi:10.1155/2015/127235
42. Gajbhiye KR, Gajbhiye V, Siddiqui IA, Gajbhiye JM. cRGD functionalised nanocarriers for targeted delivery of bioactives. *J Drug Target*. 2019;27 (2):111–124. doi:10.1080/1061186X.2018.1473409
43. Liolios C, Sachpekidis C, Kolocouris A, Dimitrakopoulou-Strauss A, Bouziotis P. PET diagnostic molecules utilizing multimeric cyclic RGD peptide analogs for imaging integrin alpha(v)beta(3) receptors. *Molecules*. 2021;26(6):1792. doi:10.3390/molecules26061792
44. Guo Q, Jin Y, Lin M, Zeng C, Zhang J. NF-kappaB signaling in therapy resistance of breast cancer: mechanisms, approaches, and challenges. *Life Sci*. 2024;348:122684. doi:10.1016/j.lfs.2024.122684
45. Conti L, Lanzardo S, Iezzi M, et al. Optical imaging detection of microscopic mammary cancer in ErbB-2 transgenic mice through the DA364 probe binding alphav beta3 integrins. *Contrast Media Mol Imaging*. 2013;8(4):350–360. doi:10.1002/cmmi.1529
46. Zhang L, Bu P. The two sides of creatine in cancer. *Trends Cell Biol*. 2022;32(5):380–390. doi:10.1016/j.tcb.2021.11.004
47. McCoy MG, Nascimento DW, Veleeparambil M, et al. Endothelial TLR2 promotes proangiogenic immune cell recruitment and tumor angiogenesis. *Sci Signal*. 2021;14(666). doi:10.1126/scisignal.abc5371
48. Ruiu R, Tarone L, Rolih V, et al. Cancer stem cell immunology and immunotherapy: harnessing the immune system against cancer's source. *Prog Mol Biol Transl Sci*. 2019;164:119–188. doi:10.1016/bs.pmbts.2019.03.008
49. Wei G, Wang Y, Yang G, Wang Y, Ju R. Recent progress in nanomedicine for enhanced cancer chemotherapy. *Theranostics*. 2021;11 (13):6370–6392. doi:10.7150/thno.57828
50. Di Lorenzo A, Bolli E, Tarone L, Cavallo F, Conti L. Toll-like receptor 2 at the crossroad between cancer cells, the immune system, and the microbiota. *Int J Mol Sci*. 2020;21(24):9418. doi:10.3390/ijms21249418
51. Quaglino E, Cavallo F, Conti L. Cancer stem cell antigens as targets for new combined anti-cancer therapies. *Int J Biochem Cell Biol*. 2020;129:105861. doi:10.1016/j.biocel.2020.105861
52. Cossu C, Di Lorenzo A, Fiorilla I, Todesco AM, Audrito V, Conti L. The role of the toll-like receptor 2 and the cGAS-STING pathways in breast cancer: friends or foes? *Int J Mol Sci*. 2023;25(1):456. doi:10.3390/ijms25010456

53. Ignacio RMC, Gibbs CR, Kim S, Lee ES, Adunyah SE, Son DS. Serum amyloid A predisposes inflammatory tumor microenvironment in triple negative breast cancer. *Oncotarget*. 2019;10(4):511–526. doi:10.18632/oncotarget.26566
54. Hubert P, Roncarati P, Demoulin S, et al. Extracellular HMGB1 blockade inhibits tumor growth through profoundly remodeling immune microenvironment and enhances checkpoint inhibitor-based immunotherapy. *J Immunother Cancer*. 2021;9(3):e001966. doi:10.1136/jitc-2020-001966
55. Yamazaki S, Okada K, Maruyama A, Matsumoto M, Yagita H, Seya T. TLR2-dependent induction of IL-10 and Foxp3+ CD25+ CD4+ regulatory T cells prevents effective anti-tumor immunity induced by Pam2 lipopeptides in vivo. *PLoS One*. 2011;6(4):e18833. doi:10.1371/journal.pone.0018833
56. Lecuyer L, Victor Bala A, Deschasaux M, et al. NMR metabolomic signatures reveal predictive plasma metabolites associated with long-term risk of developing breast cancer. *Int J Epidemiol*. 2018;47(2):484–494. doi:10.1093/ije/dyx271
57. Cimino D, Fuso L, Sfiligoi C, et al. Identification of new genes associated with breast cancer progression by gene expression analysis of predefined sets of neoplastic tissues. *Int J Cancer*. 2008;123(6):1327–1338. doi:10.1002/ijc.23660